Received: 23 January 2019 | Revised: 30 April 2020 | Accepted: 4 June 2020

DOI: 10.1096/fj.201900218R

RESEARCH ARTICLE

THE FASEB JOURNAL

Senescence-associated secretory phenotype promotes chronic ocular graft-vs-host disease in mice and humans

Mio Yamane[1] | Shinri Sato[1] | Eisuke Shimizu[1] | Shinsuke Shibata[2] | Motoshi Hayano[1] | Tomonori Yaguchi[3] | Hajime Kamijuku[4] | Mamoru Ogawa[1] | Takanori Suzuki[1] | Shin Mukai[5] | Shigeto Shimmura[1] | Hideyuki Okano[6] | Tsutomu Takeuchi[7] | Yutaka Kawakami[3] | Yoko Ogawa[1] | Kazuo Tsubota[1]

[1]Department of Ophthalmology, Keio University School of Medicine, Tokyo, Japan

[2]Electron Microscope Laboratory, Keio University School of Medicine, Tokyo, Japan

[3]Division of Cellular Signaling, Institute for Advanced Medical Research, Keio University School of Medicine, Tokyo, Japan

[4]Division of Cardiology, Department of Internal Medicine, Keio University School of Medicine, Tokyo, Japan

[5]Center for Interdisciplinary Cardiovascular Sciences, Brigham and Women's Hospital, Harvard Medical School, Boston, MA, USA

[6]Department of Physiology, Keio University School of Medicine, Tokyo, Japan

[7]Division of Rheumatology, Department of Internal Medicine, Keio University School of Medicine, Tokyo, Japan

Correspondence
Yoko Ogawa and Kazuo Tsubota, Department of Ophthalmology, Keio University School of Medicine, 35 Shinanomachi, Shinjuku-ku, Tokyo 160-8582, Japan.
Email: yoko@z7.keio.jp; tsubota@z3.keio.jp

Abstract

Chronic graft-vs-host disease (cGVHD) is a multifactorial inflammatory disease that affects patients undergoing hematopoietic stem cell transplantation. Multiple organs, including the lacrimal glands (LGs), are negatively affected by cGVHD and lose function due to the resultant fibrosis. An abnormal immune response is thought to be a major factor in the development of chronic ocular GVHD, which is currently treated primarily with immunosuppressive therapies. However, all the treatments yield unsatisfactory outcomes, and additional treatment strategies are needed. To meet this unmet medical need, we aimed to elucidate an additional pathway of chronic ocular GVHD. Our findings suggest a potential association between chronic ocular GVHD pathogenesis and stress-induced cellular senescence through the senescence-associated secretory phenotype (SASP). Senescent cells produce cytokines and chemokines, such as IL-6 and CXCL9. Indeed, senescent cell accumulation was presumably associated with cGVHD development in LGs, as evidenced by the improvement in LGs after the selective elimination of senescent cells (senolysis) with ABT-263. Results in the sclerodermatous cGVHD mouse model suggest that inhibiting the major components of the SASP, including IL-6 and CXCL9, with senolytics is a potential novel strategy for treating cGVHD-affected LGs. Taken together, our results indicate a potential association between the SASP and cGVHD development in LGs and suggest that targeted senolytic treatment may be a new therapeutic option for this disease.

Abbreviations: 53BP1, p53-binding protein 1; α-SMA, α-smooth muscle actin; BMT, bone marrow transplantation; CD, cluster of differentiation; cGVHD, chronic graftvshost disease; CXCL, chemokine (C-X-C motif) ligand; DDR, DNA damage response; ELISA, enzyme-linked immunosorbent assay; GFP, green fluorescent protein; GVHD, graft-vs-host disease; HSCT, hematopoietic stem cell transplantation; H2A.X, H2A histone family member X; HSP47, heat shock protein 47; IL, interleukin; IP, intraperitoneal; LG, lacrimal gland; miHA, minor histocompatibility antigen; OPN, osteopontin; PCR, polymerase chain reaction; RNA, ribonucleic acid; RPMI, Roswell Park Memorial Institute; SASP, senescence-associated secretory phenotype; TEM, transmission electron microscopy; TBI, total body irradiation.

Mio Yamane, Shinri Sato, Eisuke Shimizu are contributed equally to this study.

Funding information
Brain Mapping by Integrated Neurotechnologies for Disease Studies (Brain/MINDS) by Japan Agency for Medical Research and Development (AMED), Grant/Award Number: JP178dm0207002; Brain Mapping by Integrated Neurotechnologies for Disease Studies (Brain/MINDS) by Japan Agency for Medical Research and Development (AMED), Grant/Award Number: JP178dm0207001; Japanese Ministry of Education, Science, Sports, Culture and Technology, Grant/Award Number: 26462668 and 18K09421; Program for the Advancement of Research in Core Projects under Keio University's Longevity Initiative (KGRI) to K. T. and M. H.; Academic Development Project Grant-in-Aid by JSR Corporation 2019 to E. S.

KEYWORDS
chronic ocular graft-vs-host disease, lacrimal glands, senescence-associated secretory phenotype, senolytic treatment, stress-induced senescence

1 | INTRODUCTION

Hematopoietic stem cell transplantation (HSCT) is an established treatment for life-threatening hematologic malignancies. The major complication of allogeneic HSCT is graft-vs-host disease (GVHD).[1,2] Chronic GVHD (cGVHD) is a multifactorial disease characterized by immune system activation and progressive fibrosis[3] and decreases the success of allogeneic HSCT due to increased risks of death and disability.[4] Fibrosis in exocrine glands, including the lacrimal and salivary glands, as well as in the skin, lung, liver, and gastrointestinal tract is observed in cGVHD[4-6] and distinct from acute GVHD.[7] One of the most common complications is chronic ocular GVHDi.e. cGVHD-related dry eye disease, which occurs in more than 50% of cGVHD patients after HSCT and decreases quality of life.[8-11]

Progress in treating chronic ocular GVHD is hampered by the complex pathogenic mechanisms. Current treatments for chronic ocular GVHD include the local and/or systemic administration of glucocorticoids and immunosuppressants and topical lubricants, since the immune response is a major component of the pathophysiology of cGVHD. However, the response to immunosuppression remains unsatisfactory, with an overall response rate of 43%-86%.[5,12] cGVHD is observed in 10%-19% of patients after T cell-depleted HSCT.[13] Thus, effective treatment options for chronic ocular GVHD and systemic cGVHD are needed.[5,14] Although T cells are known to play important roles in the initiation of chronic ocular GVHD,[12] we hypothesize the involvement of other pathways related to stress-induced senescence.[15,16]

Previous experimental studies have explained the pathophysiology of cGVHD as regulatory T cell deficiency, thymic dysfunction, B cell activation, and cellular and cytokine network interactions.[17] Murine minor histocompatibility antigen (miHA)-disparate models have been used to investigate the pathogenesis of cGVHD, including chronic ocular GVHD.[17-19] miHA-mismatched bone marrow stromal/stem cells,[19] the tissue renin-angiotensin system,[20] and endoplasmic reticulum stress[21] are involved in the immune-mediated fibrosis in cGVHD in mice. In an animal model, macrophages in the lacrimal glands (LGs), which are affected by cGVHD, express senescence and oxidative stress markers. The senescence-related product lipofuscin accumulates in the LGs of cGVHD mice and chronologically aged mice, suggesting that cGVHD LGs undergo changes indicative of senescence.[22] Age-related changes, including the development of eyebrow and eyelash poliosis or skin wrinkles, can progress rapidly in patients with severe cGVHD.[22] Based on these findings, we hypothesized that chronic ocular GVHD is related to senescence.[23]

Cellular senescence is a stress response induced by external or internal chemical and physical insults that leads to malignant tumorigenesis by affecting checkpoint activation and inducing a stable cell cycle arrest.[24-27] Depending on the degree of stress, temporarily arrested cells can (1) transition into senescent growth arrest, (2) retain permanent damage and resume proliferation, or (3) successfully repair damage and resume normal cell cycle progression.[26]

Senescent cells not only can live for a long time, but also irreversibly arrest the cell cycle and secrete substances, including inflammatory cytokines and chemokines, that promote chronic inflammation; this condition is termed the senescence-associated secretory phenotype (SASP).[25,27] SASP is the major downstream mediator of cellular senescence.[25,28] Interleukin (IL)-1β, IL-6, IL-8, CXCL1, and CXCL9 are reported to be major components of the SASP.[25,27,29] Moreover, IL-6 is known to play a critical role in cGVHD progression.[19,30,31] In the cGVHD mouse model, the mice undergo total body irradiation (TBI) and

allogeneic BMT, both of which may accelerate cellular senescence in these animals compared with syngeneic controls beyond that expected from conventional immune responses alone.[22]

This study aimed to determine whether cGVHD-affected LGs show signs of stress-induced senescence and release cytokines and chemokines, the major components of the SASP. In addition, we aimed to confirm that the selective elimination of senescent cells (senolysis) by ABT-263[28,32,33] improves LGs affected by cGVHD.

2 | MATERIALS AND METHODS

2.1 | Mice

B10.D2/nSnSlc and BALB/cCrSlc mice (7-9 weeks old) were purchased from Sankyo Laboratory, Inc (Tokyo, Japan). GFP mice were obtained by backcrossing B10.D2/nSnSlc mice with C57BL/6 GFP mice (Japan SLC Ltd, Shizuoka, Japan). Progeny of the 10th generation of backcrossed B10.D2/nSnSlc GFP were used for the experiments.

2.2 | Whole bone marrow transplantation (BMT)

To generate the cGVHD mouse model, allogeneic BMT was performed with 7- to 9-week-old male B10.D2/nSnSlc and female BALB/cCrSlc mice as transplant donors and recipients, respectively, as previously reported, representing MHC-compatible, miHA-mismatched BMT. As a non-cGVHD control, syngeneic BMT was conducted by transplanting donor cells from male BALB/cCrSlc mice into female BALB/cCrSlc mice, which were irradiated with 7 Gy of X-ray using a Gammacell 137Cs source (Hitachi Medico, Ltd, Tokyo, Japan). Donor cells (1×10^6 bone marrow cells/mouse and 2×10^6 spleen cells/mouse) were suspended separately in 100 μL of RPMI1640 medium, and then, combined. This 200-μL suspension was injected into the recipient via the tail vein.[18] The recipient animals were maintained in sterile cages and given autoclaved food and acidified water. The cGVHD and non-cGVHD control mice were used for experiments at 2, 3, 4, or 8 weeks after BMT.

2.3 | Treatment of allogeneic BMT recipient mice with ABT-263

Allogeneic BMT recipient mice were divided into 2 groups; one was treated with ABT-263 (Navitoclax, S1001, Selleck Chemicals, Houston, TX), and the other was given solvent vehicle. Mice were treated daily for 7 consecutive days starting 10 days after BMT by gavage with either 50 mg/kg, 25 mg/kg, 12.5 mg/kg of ABT-263 or vehicle (ethanol [Sigma-Aldrich, St. Louis, MO], polyethylene glycol 400 [HR2-603, Hampton Research, Aliso Viejo, CA], and Phosal 50 PG [H. Holstein, Hamburg, Germany] at a percentage ratio of 10:30:60).[28,32,34] Mice were analyzed 28 days after BMT.

2.4 | Treatment of allogeneic BMT recipient mice with anti-mouse IL-6 receptor (anti-IL-6R) monoclonal antibody (mAb)

Allogeneic BMT recipient mice were divided into 2 groups; one was treated with MR16-1 (Tocilizumab, Chugai, Tokyo, Japan), a humanized mAb specific for IL-6R, and the other was given vehicle (PBS, pH 7.4). The anti-IL-6R mAb or PBS was administered by IP injection at 2 mg/mouse 1 day before and at 0.5 mg/mouse 10, 17, and 24 days after BMT.[35] The mice were analyzed 28 days after BMT.

2.5 | In vivo imaging

To detect myeloperoxidase activity of activated phagocytes such as macrophages in deep tissues in vivo, mice were anesthetized and received an IP injection of XenoLight RediJect Inflammation Probe (760535, PerkinElmer, Waltham, MA), a chemiluminescent reagent for monitoring inflammation, at 200 mg/kg 10 minutes before beginning the photon recording. The mice were placed in a dark box, and luminescence images were acquired using an electron multiplying CCD camera (C9100-13, Hamamatsu Photonics KK, Hamamatsu, Japan).[36]

2.6 | Histological analysis

Mice were sacrificed by cervical dislocation 3, 4, or 8 weeks after BMT. The LGs and skin were harvested and fixed with 20% neutralized buffered formalin overnight, embedded in paraffin wax, and processed for H&E and Mallory staining.[19,20] To quantify the fibrotic areas[20,37] in the LGs and skin in tissue sections, images were acquired at 400 times magnification, and 3 images of the LGs and skin from each Mallory-stained section were examined. These images were analyzed using Color Deconvolution, a plugin for Image J, with which we separated the colors of each image into blue, green, and red. The area of blue color was measured using the same threshold.[38] The average value obtained from the 3 images from each sample was regarded as the value for the fibrotic area.

2.7 | Immunohistochemistry using whole-mount lacrimal glands

Mice were sacrificed, after which the LGs were removed using sterile technique and minced into small pieces using a scalpel. The tissue pieces were washed, incubated in BD CellFIX (340181, BD Pharmingen, San Diego, CA) for 1 hour at room temperature, and permeabilized with 0.2% of Triton X-100 (3501-02, Nacalai tesque, Kyoto, Japan) for 10 minutes. The specimens were then blocked with 10% of normal goat serum (50062Z, Thermo Fisher Scientific, Waltham, MA) for 30 minutes and incubated with optimally diluted primary antibodies specific to CD4 (14-0042-81, RM4-5, eBioscience, San Diego, CA) and CD153 (14-1531-85, RM153, eBioscience) overnight at 4°C, and then, with an Alexa Fluor 488-conjugated goat anti-rat IgG secondary antibody (A11006, Thermo Fisher Scientific) and DAPI (D21490, Thermo Fisher Scientific) for 45 minutes at room temperature to stain the nuclei, as described previously.[39] Isotype antibodies including rat IgG2a, κ (14-4321-82, eBR2a, eBioscience) for CD4 and rat IgG2b, κ (14-4031-82, eB149/10H5, eBioscience) for CD153 were used as negative controls. The samples were mounted with Fluorescent Mounting Medium (S3023, Agilent Technologies, Santa Clara, CA) on a glass slide and covered with a cover glass (C024241, Matsunami Glass, Osaka, Japan). Fluorescence images were captured with an LSM 700 or LSM 710 confocal microscope (Carl Zeiss, Jena, Germany).

2.8 | Immunostaining of frozen tissue sections

Immunohistochemical analyses were performed as described previously.[19] The LG tissues were embedded in optimal cutting temperature (OCT) compound (4583, Sakura Finetek, Torrance, CA) in precooled isopentane and stored at −80°C until cutting into 6-μm-thick sections. The sections were fixed in acetone for 20 minutes at room temperature, rehydrated in PBS, and blocked with 10% of normal goat serum for 30 minutes at room temperature. In some experiments for single staining, the sections were incubated overnight at 4°C with optimally diluted primary antibodies. The primary antibodies used for the LGs from human samples were 53BP1 (SC-22760, H-300, Santa Cruz Biotechnology, Dallas, TX), IL-8 (ab18672, 807, Abcam, Cambridge, United Kingdom), and IL-6 (ab6672, Abcam). Next, the sections were incubated for 45 minutes at room temperature with DAPI and the secondary antibodies. Each step was followed by three washes with PBS. In some experiments using mouse LGs, the tissue sections were double stained with Bax (active monomer) (ALX-804-224-C100, 6A7, Enzo Life Science, Farmingdale, NY) or Cleaved Caspase-3 (9661, Cell Signaling Technology, Danvers, MA). In some experiments using mouse LGss, acetone-fixed the tissue sections were double stained with(1) purified p16 (sc-1207, M-156, Santa Cruz Biotechnology) and CXCL1 (ab17882, polyclonal, Abcam) or (2) CXCL9 (ab137792, polyclonal, Abcam) and APC-labeled CD68 (137007, FA-11, BioLegend, San Diego, CA) overnight at 4°C. After being washed, the sections were incubated for 45 minutes at room temperature with DAPI and the secondary antibodies. For double staining using fluorophore-conjugated primary antibodies, PE-labeled MHC class II (12-5321, M5/114.15.2, eBioscience) or PE-labeled IL-6(554401, MP5-20F3, BD Pharmingen) and either APC-labeled CD3 (17-0031, 145-2C11, eBioscience), APC-labeled CD68, or APC-labeled CD154 (17-1541, MR1, eBioscience) were co-stained over night at 4°C. After being washed, the sections were incubated for 45 minutes with DAPI. For triple staining, the tissue sections were stained with Osteopontin (OPN) (O7635, polyclonal, Sigma-Aldrich), APC-labeled CD279 (PD-1) (109111, RMP1-30, eBioscience), and either CD4 (14-0042-81, RM4-5, eBioscience) or PE-labeled CD153(137007, FA-11, BioLegend) over night at 4°C. After being washed, the sections were incubated with DAPI and secondary antibodies for 45 minutes at room temperature. In other experiments for double staining using same species for two primary antibodies, acetone-fixed tissue sections were stained with PE-labeled MHC class II and CD40 (124601, 3/23, BioLegend) in combination with Alexa Fluor 647-conjugated goat anti-rat IgG secondary antibody (A21247, Thermo Fisher Scientific) by two steps. The sections were incubated overnight at 4°C with optimally diluted the conjugated primary antibody as a first reaction, and then, for two hours at room temperature with optimally diluted purified primary antibodies as a second reaction. Next, the sections were incubated for 45 minutes with DAPI and the secondary antibodies.[40] The secondary antibodies used were (1) Alexa Fluor 488-conjugated goat anti-rabbit IgG secondary antibody (A11034, Thermo Fisher Scientific) for p16, CXCL1, CXCL9, 53BP1, and IL-8; (2) Alexa Fluor 488-conjugated goat anti-mouse IgG secondary antibody (A11029, Thermo Fisher Scientific) for IL-8; (3) Alexa Fluor 568-conjugated goat anti-rat IgG secondary antibody (A11077, Thermo Fisher Scientific) for CD68; (4) Alexa Fluor 647-conjugated goat anti-hamster IgG secondary antibody (127-605-160, Jackson ImmunoResearch Laboratories, West Grove, PA) for CD3 and CD154; (5) Alexa Fluor 488-conjugated rabbit anti-goat IgG secondary antibody (A11078, Thermo Fisher Scientific) for IL-1β and OPN; (6) Alexa Fluor 568-conjugated goat anti-rabbit IgG secondary antibody (A11011, Thermo Fisher Scientific) for Cleaved Caspase-3; (7) Alexa Fluor 568-conjugated goat anti-mouse IgG secondary antibody (A11004, Thermo Fisher Scientific) for Bax (active monomer); (8) Alexa Fluor 660-conjugated goat anti-rabbit IgG secondary antibody (A21074, Thermo Fisher Scientific) for CD4. Isotype-matched antibodies used as negative controls were (1) rabbit IgG antibody (2729, Cell Signaling Technology) for

p16, 53BP1, CXCL1, CXCL9, IL-8, and Cleaved Caspase-3; (2) rat IgG2a antibody (MAB006, 54447, R&D Systems, Minneapolis, MN) for CD68; (3) APC-labeled rat IgG2b, κ antibody (400611, RTK4530, BioLegend) for MHC class II; (4) APC-labeled rat IgG2a, κ antibody (400611, RTK4530, BioLegend) for CD68; (5) Armenian hamster IgG antibody (14-4888, eBioscience) for CD3 and CD154; (6) rat IgG2a, κ antibody for CD40; (7) PE-labeled Rat IgG1, λ antibody and (8) mouse IgG1, κ (14-4714-82, P3.6.2.8.1, eBioscience) for IL-8 and Bax (active monomer); (9) PE-labeled rat IgG1, κ antibody (401905, BioLegend) for IL-6.

2.9 | Immunostaining of formalin-fixed paraffin-embedded tissue sections

After deparaffinization and dehydration, target antigens were unmasked using microwave method at 100ºC for 10 minutes for p16 (sc-1661, F-12, Santa Cruz Biotechnology), Caspase-1 (06-503-I, polyclonal, EMD Millipore Corporation, Temecula, CA), IL-1β (AF-401-NA, polyclonal, R&D Systems), IL-8 (BS3479, polyclonal, Bioworld Technology, St. Louis Park, MN), CXCL1 (ab17882, polyclonal, Abcam), IL-6, CXCL9 (ab137792, polyclonal, Abcam), CD68, CD45 (550539, 30-F11, BD Pharmingen), OPN(O7635, polyclonal, Sigma-Aldrich), and α-SMA (ab7817, 1A4, Abcam) or autoclave methods at 120ºC for 20 minutes for γ-H2A.X (9718, 20E3, Cell Signaling Technology), 53BP1, p21 (ab2961, polyclonal, Abcam), Ki-67 (RM-9106, SP6, Abcam), and HSP47 (SPA-470, M16.10A1, Stressgen Biotechnologies, Victoria British Columbia, Canada) in target retrieval solution (S169984, Agilent Technologies). The sections were blocked with 10% of normal goat serum or normal rat serum (012-000-120, Jackson ImmunoResearch Laboratories) for 30 minutes at room temperature and incubated overnight at 4°C with optimally diluted primary antibodies. The primary antibodies used for mouse samples were γ-H2A.X; 53BP1; p16; p21; Ki-67; Caspase-1; IL-1β; IL-8; CXCL1; IL-6; CXCL9; CD68; CD45; OPN; HSP47; and α-SMA. The sections were then incubated for 45 minutes at room temperature with DAPI and the secondary antibodies including (1) Alexa Fluor 488-conjugated goat anti-rabbit IgG secondary antibody for γ-H2A.X, 53BP1, p21, Ki-67, Caspase-1, IL-8, CXCL1, IL-6, CXCL9, and Ki-67; (2) Alexa Fluor 488-conjugated goat anti-mouse IgG secondary antibody for p16, HSP47, and α-SMA; (3) Alexa Fluor 488-conjugated goat anti-rat IgG secondary antibody for CD68, and CD45; (4) Alexa Fluor 488-conjugated rabbit anti-goat IgG secondary antibody (A11078, Thermo Fisher Scientific) for IL-1β and OPN; (5) Alexa Fluor 568-conjugated goat anti-rat IgG secondary antibody for CD68; and (6) Alexa Fluor 568-conjugated goat anti-mouse IgG secondary antibody (A11031, Thermo Fisher Scientific) for α-SMA. In some experiments, the co-expression of IL-6 and CD68 or of CXCL9 and α-SMA on the LGs was examined by double staining methods as described previously.[19] Isotype-matched antibodies used as negative controls were (1) rabbit IgG antibody for γ-H2A.X, 53BP1, p21, Ki-67, Caspase-1, IL-8, CXCL1, IL-6, CXCL9, and Ki-67; (2) mouse IgG2a antibody for p16; (3) rat IgG2a antibody for CD68; (4) goat IgG antibody for IL-1β and OPN; (5) rat IgG2b, κ antibody for CD45; (6) mouse IgG2b antibody for HSP47; and (7) mouse IgG2a, κ antibody for α-SMA. The number of target cells per field was quantified by averaging at least five non-overlapping fields for each section. To estimate the histological architecture and staining, each slide was observed three times by two independent observers (MY and YO). Image J was used to analyze the CXCL9- and OPN-positive areas in vessels at 200 times magnification.[38] Five images of the LGs for each sample were analyzed, and the colors of each image were separated into blue, green, and red. The area of green color was measured using the same threshold. The mean value obtained from 5 images for each sample was regarded as the value for the CXCL9- and OPN-positive areas.

2.10 | Apoptosis assay

Apoptosis was assayed with a fluometric TUNEL system (G3250, Promega, Madison, WI) as described previously.[41] Each step was followed by three washes with PBS. The frozen sections were fixed by immersing slides into freshly prepared 4% of methanol-free formaldehyde in PBS for 25 minutes at 4°C and permeabilized by immersing the slides into 0.2% of Triton X-100 in PBS for 5 minutes. The frozen sections were covered with 100 μL Equilibration Buffer and equilibrated at room temperature for 10 minutes. For the experimental reactions, an incubation buffer was prepared by combining Equilibration Buffer (45 μL), Nucleotide Mix (5 μL), and rTdT Enzyme (1 μL). Cleaning wipes (Kimberly-Clark Corp., Irvine, TX) were used to blot the areas around the equilibrated tissues, and 50 μL incubation buffer was added to a 5 cm^2 area of the frozen sections. The slides were incubated at 37°C for 60 minutes in a humidifying light-blocking chamber. The reaction was stopped by immersing the slides into 2× saline sodium citrate buffer for 15 minutes at room temperature. The sections were incubated with DAPI at room temperature for 15 minutes.

2.11 | Immunocytochemistry of cultured fibroblasts derived from lacrimal glands in mice

LG fibroblasts from cGVHD and syngeneic control recipient mice were cultured as described previously.[42] Briefly, LG tissue was minced with sterilized scissors into small pieces, and transferred to plates containing DMEM supplemented with penicillin (200 U/mL), streptomycin (200 U/mL), and

10% of fetal bovine serum for fibroblast growth. Cultures were maintained at 37°C in a humidified atmosphere of 5% of CO_2 and 95% of air. The medium was replaced with fresh medium every 3 days. Confluent cells were detached by incubation with 0.05% of trypsin for 1.5 minutes and centrifuged (400 ×*g* for 10 minutes at 4°C). The cell pellet was then resuspended in DMEM. LG fibroblast cultures were performed 3 times. The LG fibroblast cultures were used between the third and seventh passages. In addition, fibroblasts were cultured on fibronectin-coated chamber slides (354631, Corning, Corning, NY), fixed on the slide with 10% of neutral-buffered formalin (20211, Muto Pure Chemicals, Tokyo, Japan) for 30 minutes at room temperature, and incubated for 2 hours at room temperature with optimally diluted primary antibodies. Primary antibodies used for cultured fibroblasts were 53BP1, p16, Ki-67, and HSP47. The negative controls used were as described previously.[19] The chambers were then incubated for 45 minutes at room temperature with DAPI and the secondary antibodies including (1) Alexa Fluor 660-conjugated goat anti-rabbit IgG secondary antibody (A21074, Thermo Fisher Scientific) for 53BP1; (2) Alexa Fluor 488-conjugated goat anti-rabbit IgG secondary antibody for p16; (3) Alexa Fluor 488-conjugated goat anti-rabbit IgG secondary antibody for Ki-67; and (4) Alexa Fluor 568-conjugated goat anti-mouse IgG secondary antibody for HSP47.

2.12 | Transmission electron microscopy (TEM)

We examined under an electron microscope (1230 EXII and model 1400plus JEOL, Tokyo, Japan). Electron micrographs were acquired with a BioScan camera (Gatan BioScan camera model 792, Roper Technologies, Sarasota, FL).

2.13 | RNA isolation and real-time quantitative polymerase chain reaction

Total RNA was performed as described previously42. Extracted from extra-orbital LGs using a miRNeasy mini kit (217004, Qiagen, Valencia, CA), and complementary DNA was synthesized using a ReverTra Ace qPCR RT Kit (FSQ-101, Toyobo, Osaka, Japan). Real-time qPCR was performed using the StepOnePlus system (4379216, Thermo Fisher Scientific). The primers used for qPCR, including Mm00515990_s1 for H2afx, Mm01271863_m1 for Trp53bp1, Mm00494449_m1 for Cdkn2a (p16), Mm04205640_g1 for Cdkn1a (p21), Mm00434228_m1 for Il1b, Mm00446190_m1 for Il6, Mm00434946_m1 for Cxcl9, Mm00483888_m1 for Col1a2, and Mm01178820_m1 for Tgfb1, were purchased from Applied Biosystems/Thermo Fisher Scientific. All data were analyzed using the $2^{-\Delta\Delta CT}$ method, and the housekeeping gene GAPDH was used as the internal standard to measure the expression of mRNA. The experiments were performed in triplicate.

2.14 | ELISA

Serum was collected from mice using cheek venipuncture and humans using blood sampling from vein. The concentration of IL-6 in the supernatants was determined by ELISA using a specific kit, according to the manufacturer's instructions (M6000B for mouse and D6050 for human, R&D Systems). The experiments were performed in triplicate.

2.15 | Isolation and co-culture of T cells and macrophages

Spleens were obtained from 4 cGVHD mice and 4 syngeneic control ones 4 weeks after BMT. T cells and macrophages were purified from the spleens with anti-CD90.2 monoclonal antibody (mAb)-conjugated microbeads (130-110-443, Miltenyi Biotic, Bergisch Gladbach, Germany) or anti-F4/80 mAb-conjugated microbeads (130-110-443, Miltenyi Biotic), respectively, according to the manufacturer's instructions. T cells and macrophages were co-cultured in RPMI at a ratio of 10:1 (T cells: 10^5 cells per well, macrophages: 10^4 cells per well) for 4 days in a 96-well plate. The suspension cells were collected, and the adherent cells were harvested using a cell detachment solution (C5914, Sigma-Aldrich). These collected cells were stained with fluorophore-conjugated antibodies and analyzed by flow cytometry as described below.

2.16 | Flow cytometry analysis

Spleens were harvested from cGVHD mice and syngeneic control ones 4 weeks after BMT. The splenocytes from the cGVHD mice were pooled, and the same was applied to those from the syngeneic control ones. In some experiments, GFP-transgenic mice were used as donors in order to distinguish donor- from recipient-derived cells, and the spleen cells were stained with anti-mouse CD68 and anti-mouse IL-6 antibodies. In other experiments, the spleen cells were stained with anti-mouse CD68, anti-mouse IL-6, and anti-mouse p16 antibodies. Single-cell suspensions of splenocytes were prepared by mashing spleens with the rubber end of a plunger from a 2.5 mL syringe through a 40 μM Nylon filter (352340, BD Falcon, Bedford, MA, USA). Hemolysis was performed using ACK lysis buffer (5 mL/spleen) (118-156-721EA,

Quality Biological, Inc, Gaithersburg, MD). The cells were then washed with PBS and stained with APC-labeled anti-mouse CD68 antibody (137007, FA-11, BioLegend) for 30 minutes on ice. Next, the cells were washed with PBS, permeabilized and fixed with a fixation/permeabilization solution (554714, BD Pharmingen) for 10 minutes on ice. After being washed with perm/wash buffer (554714, BD Pharmingen) twice, the cells were then incubated with PE-labeled anti-mouse IL-6 antibody (554401, MP5-20F3, BD Pharmingen) and p16 antibody (sc-1207, M-156, Santa Cruz Biotechnology) for 30 minutes on ice. The cells were washed with the perm/wash buffer twice and stained with Alexa Fluor 488-conjugated goat anti-rabbit IgG secondary antibody (A11034, Thermo Fisher Scientific) for 30 minutes on ice. After being washed with the perm/wash buffer, the cells were suspended in staining buffer (FC001, R&D Systems, Minneapolis, MN). Isotype-matched antibodies used as negative controls were (1) rabbit IgG antibody (2729, Cell Signaling Technology) for p16; (2) APC-labeled rat IgG2a, κ antibody (400611, RTK4530, BioLegend) for CD68; (3) PE-labeled rat IgG1, κ antibody (401905, BioLegend,) for IL-6. The stained cells were analyzed using a flow cytometer (Gallios, Beckman Coulter Life Sciences, Indianapolis, IN), and the data were analyzed with software designed for the cytometer (Kaluza Analysis Software, Beckman Coulter Life Sciences, Indianapolis, IN).

2.17 | Fluorescein staining on the ocular surface

Four weeks after BMT, the recipient mice were evaluated for corneal epithelitis. One microliter of 0.5% of fluorescein sodium solution (Fluorescite, 877290, Novartis Pharma, Tokyo, Japan) was instilled into the temporal conjunctival sac without anesthesia. The ocular surface was observed under cobalt blue light using a microscope (SZ61, Olympus, Tokyo, Japan).

2.18 | Cotton thread test for measuring tear secretion

A phenol red thread (Zone-Quick; 2564187, Showa Yakuhin Kako Co., Ltd., Tokyo, Japan) was placed on the temporal side of the lower eyelid margin for 15 seconds. The length of moistened thread from the end was measured for both eyes, and the average was used as the tear volume.[42] This procedure was performed three times on each of three consecutive days before BMT and day 27 after BMT. The average of the three measurements was used as the tear volume of each mouse at each time point.

2.19 | Biopsy of lacrimal gland specimens from patients

For the purpose of diagnosis, LG biopsy was performed for patients with cGVHD and IgG4-related disease. The remaining LG specimens were used for this study.[40,43] As cGVHD samples, we used the LGs from patients who had received HSCT and in whom dry eye disease developed later. The LGs from patients with IgG4-related disease were used as disease control samples.

2.20 | Diagnosis of the cGVHD-related dry eye disease in humans

Patients who experienced newly developed dry eye disease after HSCT were considered to have cGVHD if they met all three of the following criteria: (1) the symptoms of dry eye disease; (2) positive fluorescein staining (equal to or over 3 on a scale of 0 to 9) and/or rose bengal staining (equal to or over 3 on a scale of 0 to 9); and (3) a Schirmer I test value of 5 mm or less and/or tear-film breakup time of 5 seconds or less.[2] Patients in whom dry eye disease was not diagnosed after HSCT were regarded as non-cGVHD.

2.21 | Photographs of eyes of cGVHD patients

We followed up the HSCT patients at the dry eye outpatient clinic and recorded their ocular findings before and after HSCT collaborating with the KEIO BMT program transplant internist. Photographs of the anterior ocular segments from a cGVHD patient (58 years old female) were taken by a slit-lamp microscope device (BQ 900, HAAG-STREIT AG, Koeniz, Switzerland).

2.22 | Statistical analysis

Data were analyzed by the two-tailed unpaired Student's *t* test or Welch's *t* test. Two-sided *P* values less than .05 were considered significant. The data are presented as the mean ± SEM. Statistical analyses were performed using both Microsoft Excel 2013 and R 3.4.2 (R Foundation for Statistical Computing, Vienna, Austria), and both methods yielded the same results.

2.23 | Study approval

For the human study, written informed consent was obtained from all participants prior to study participation. The

institutional research ethics committee of Keio University School of Medicine approved this study (No. 20090277), and this study adhered to the tenets of the Declaration of Helsinki. For the animal study, all the experimental procedures were in accordance with the Institutional Guidelines on Animal Experimentation at Keio University and the ARVO Statement for the Use of Animals in Ophthalmic and Vision Research. Our animal protocols were approved by the Keio University Institutional Animal Care and Use Committee (# 09152).

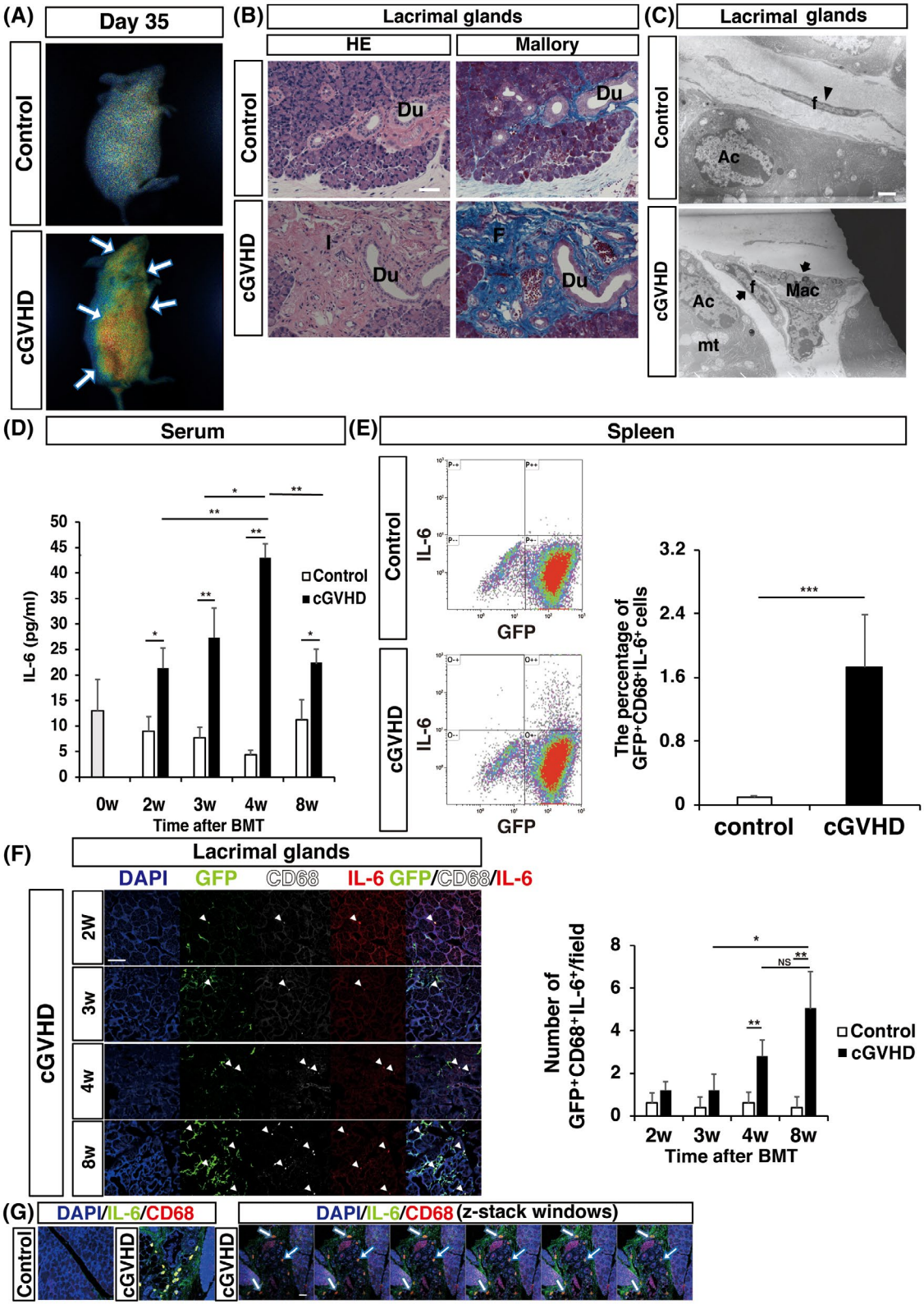

FIGURE 1 Activated macrophages in the lacrimal gland and the time course of IL-6 elevation in the serum of cGVHD mice. *A*, Myeloperoxidase activity in cGVHD and control mice after disease onset revealed by imaging using the XenoLight RediJect inflammation probe. The cGVHD mice showed severe inflammation, which correlated with increased chemiluminescence in the LGs, salivary glands, skin, lungs, liver, and intestine (white arrows). *B*, H&E (left) and Mallory (right) staining of murine cGVHD (lower row) and control (upper row) LGs. Du, duct; I, inflammatory cells; F, fibrosis. Scale bar: 50 μm. *C*, Electron microscopic images showing an activated fibroblast attached to a macrophage in the cGVHD LGs (black arrow) and a quiescent fibroblast in the control LGs (black arrowhead). Ac, acinar cell; f, fibroblast; Mac, macrophage; mt, mitochondria. Scale bar: 1 μm. *A-C*, Data are representative of at least two independent experiments (n = 3 per group). *D*, Serum IL-6 levels in recipient mice of the cGVHD and control groups before and 2, 3, 4, and 8 weeks after BMT (n = 4 per group). Data are presented as the mean ± SEM. *$P < .05$, ** $P < .01$, unpaired Student's *t* test. BMT, bone marrow transplantation. *E*, Flow cytometric analysis of IL-6-producing donor-derived GFP^+ and recipient-derived GFP^- macrophages among spleen cells. ***$P < .001$, unpaired Student's *t* test. Data are presented as the mean ± SEM *F*, Double staining for IL-6 (red) and CD68 (white) in cGVHD and control LGs 2,3,4 and 8 weeks after BMT (white arrows indicate $GFP^+IL\text{-}6^+CD68^+$ cells). The three colors in each image are shown individually. *F* (right), Time-dependent evaluation of IL-6-producing GFP^+ macrophages in cGVHD LGs. *$P < .05$, ** $P < .01$, unpaired Student's *t* test. Data are presented as the mean ± SEM *G*, Double staining for IL-6 (green) and CD68 (red) in cGVHD and control LGs 8 weeks after BMT. Representative images are shown (cGVHD, n = 1 and 9 fields; control, n = 1 and 11 fields). Z-stack (1 μm) images of cGVHD LGs.

3 | RESULTS

3.1 | Activated macrophages in a cGVHD mouse model

To examine whether cGVHD-related immune processes are related to SASP, we used an established sclerodermatous cGVHD mouse model.[18,19] Macrophages in the LGs of this model express the senescence biomarkers p16 and p38 and oxidative stress markers.[22]

We first analyzed whether the activity of the inflammation marker myeloperoxidase (MPO) was elevated in cGVHD. Imaging using the XenoLight RediJect inflammation probe showed that MPO activity was increased in cGVHD model recipients but not controls 35 days after BMT, which is after the onset of disease (Figure 1A). In addition, activated macrophages infiltrated target organs, including the LGs, skin, lungs, liver, and intestine, in cGVHD mice 35 days after BMT (Figure 1A).

We next focused on the LGs, one of the most frequently affected organs in cGVHD.[19,44,45] Compared with the LGs of syngeneic controls, those of allogeneic BMT recipients (cGVHD) had more inflammatory cells and larger fibrotic areas (Figure 1B), as described previously.[46] Ultrastructural analysis revealed activated fibroblasts attached to macrophages in the cGVHD LGs (Figure 1C). Immunofluorescence showed that a subpopulation of macrophages expressing MHC class II and CD40 derived from GFP-positive donor cells exhibited the phenotype of antigen-presenting cells, which activated a subset of $CD154^+$ T cells in cGVHD LGs but not control LGs (Supplemental Figure S1*A,B*).[19] In addition, serum IL-6 levels were significantly higher in cGVHD mice than in control mice starting at 2 weeks, and these levels gradually increased until 4 weeks after BMT (Figure 1D). Notably, the increase in serum IL-6 coincided with increases in tissue inflammation and fibrosis in cGVHD LGs. Donor-derived macrophages from the spleen produced more IL-6 in cGVHD mice than in syngeneic controls (Figure 1E). IL-6-producing donor-derived macrophages accumulated in a time-dependent manner in cGVHD-affected LGs (Figure 1F, G).

These observations suggested that interactions among donor-derived IL-6-producing macrophages, T cells, and fibroblasts contribute to LG pathology in cGVHD mice but not controls.

3.2 | Relationship between cGVHD and SASP-related molecules

Senescent cells are characterized by (1) the DNA damage response (DDR), (2) p16-RB and/or p53 pathway activation and irreversible cell cycle arrest, and (3) the secretion of SASP-related factors.[15,24,26] To determine whether senescent cells with these characteristics are present in cGVHD LGs, we firstly analyzed the mRNA and protein expression of molecules related to (1) the DDR, (2) senescence, and (3) the SASP in cGVHD LGs.

The mRNA expression of CXCL9, a major component of the SASP, was significantly elevated in cGVHD LGs compared with control LGs (Supplemental Figure S2).

During the early stage of disease in cGVHD LGs, infiltrated interstitial cells surrounding the ducts and in the stroma expressed markers of the DDR (53BP1), DNA double-strand breaks (ɤ-H2A.X), and cell proliferation (Ki67)[27,29,32,47] (Figure 2A), as well as the senescence biomarkers p16 (Figure 2B, right, quadrant images) and p21 (Figure 2B, left).[15] The LGs of cGVHD mice had significantly more $p16^+CD68^+$ macrophages than those in syngeneic control mice, indicating the presence of senescent macrophages in the cGVHD LG microenvironment (Figure 2B, quadrant image). The number of cells/field expressing p16, Ki67, and CD68 was higher for cGVHD LGs than control LGs (Figure 2*A,B*), indicating that cGVHD LGs contain DNA-damaged senescent cells. We further confirmed

a significantly higher percentage of p16 expressing cells (Figure 2C, upper right) and IL-6$^+$ p16$^+$ cells (Figure 2C lower right) in total CD68$^+$ macrophages in the spleen of cGVHD mice than that of syngeneic controls (Figure 2C). We next examined whether DNA-damaged cells in cGVHD LGs secrete SASP-related factors, including caspase-1 (an essential component of the inflammasome that processes IL-1β[48]) (Figure 2D left), IL-1β (a marker of upstream SASP induction),[47] and IL-8 (a subsequent product) (Figure 2D, middle).[47] Among inflammatory cells, CXCL1$^+$CD68$^+$ and

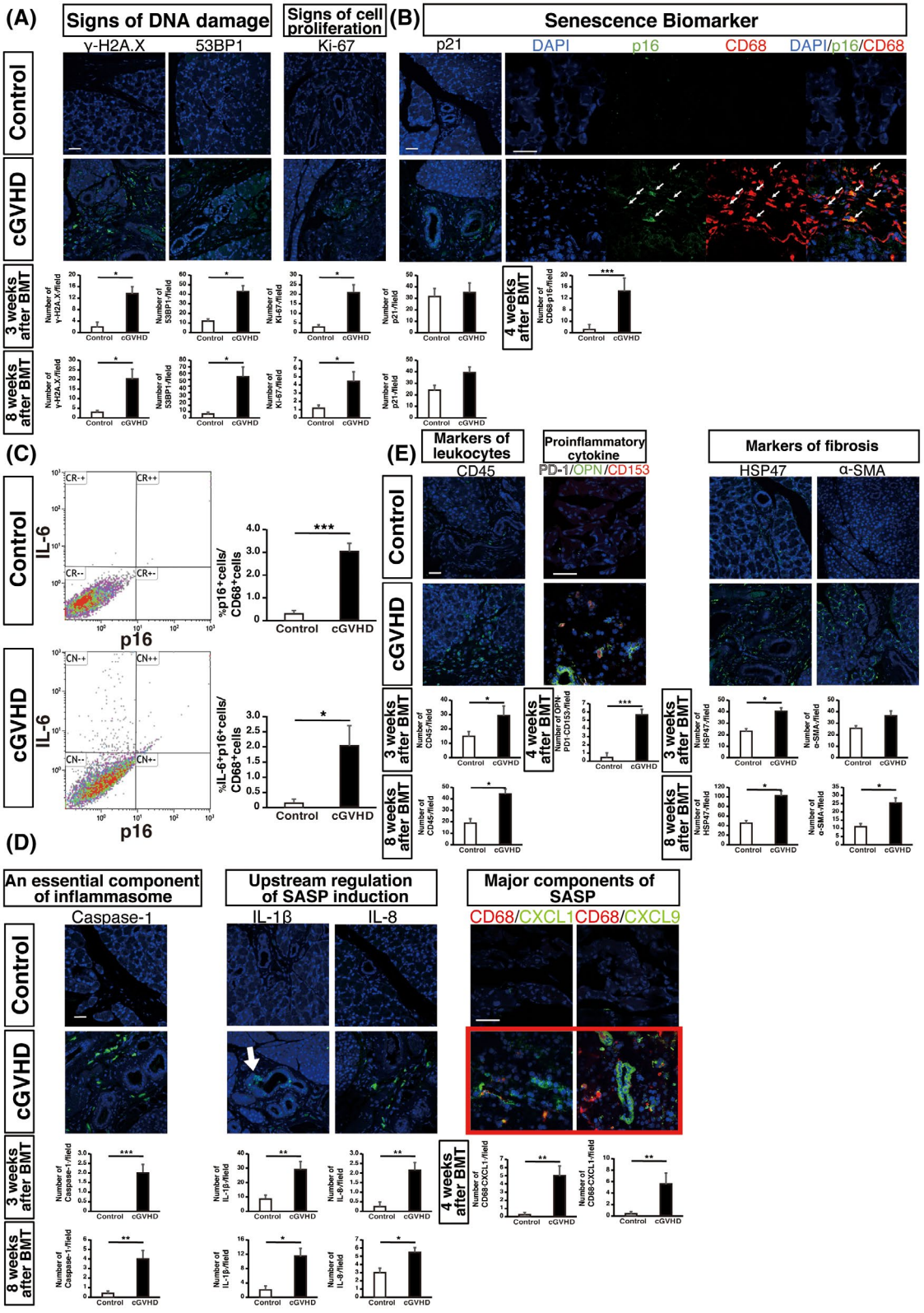

FIGURE 2 SASP-related molecules are elevated in cGVHD lacrimal glands. *A, B*, Lacrimal gland (LG) sections from cGVHD and control mice 3 and 8 weeks after bone marrow transplantation (BMT) were stained for ɤ-H2A.X and 53BP1 (DNA damage response, green, *A*), Ki-67 (proliferation, green, *A*) and p21 (senescence, green, *B*). *B*, Lacrimal gland (LG) sections from cGVHD and control mice 4 weeks after bone marrow transplantation (BMT) were stained for p16 (senescence) and CD68 (macrophage). Colocalization of p16 (green) and CD68 (red) (arrows) shown by quadrant image (*B*, right). *C*, Flow cytometric analysis of IL-6 and p16-expressing $CD68^+$ cells. *P<.05. *D*, Caspase-1 (inflammasome, green), IL-1β and IL-8 (upstream of SASP induction, green), and CXCL1 and CXCL9 (SASP components). Colocalization of CD68 (red) and CXCL1 or CXCL9 (green). IL-$1\beta^+$ cells on the ducts are indicated by white arrows. *E*, The leukocyte marker CD45 (green) and the fibrosis markers HSP47 and α-SMA (green); colocalization with senescent T cell markers (PD1, white; CD153, red) and a SASP marker (OPN, green). The number of $PD1^+CD153^+OPN^+$ cells per field of the LG 4 weeks after BMT. Data are representative of three (8 weeks after BMT) or one (3 and 4 weeks after BMT) independent experiment (n = 3 or 4 per group;> 5 fields). A-E, Data are presented as the mean ± SEM. *P < .05, ** P < .01, *** P < .001, unpaired Student's t test. DAPI stains nuclei blue. Scale bar: 50 μm

$CXCL9^+CD68^+$ double-positive cells (macrophages expressing major SASP components)[25] were more populous in cGVHD LGs than in control LGs (Figure 2D, right). The numbers of caspase-1^+, IL-$1\beta^+$, IL-8^+, $CXCL1^+CD68^+$, and $CXCL9^+CD68^+$ cells per area were significantly higher in the cGVHD group than in the control group (Figure 2D). In particular, IL-1β was more highly expressed on LG ducts in cGVHD mice than in control mice (Figure 2D, arrow). More $CD45^+$ inflammatory cells infiltrated cGVHD LGs than control LGs (Figure 2E, left). Previous reports showed that $CD153^+PD1^+CD4^+$ T cells express a cellular senescence signature and secrete pro-inflammatory cytokines, including OPN,[39] a known SASP factor[49] and profibrotic molecule upregulated by IL-6 trans-signaling[50] that regulates epithelial-mesenchymal transition[51] and is expressed in various tissues and cells.[52] The number of OPN^+ cells in the LGs was significantly higher in the cGVHD group than the control group (Figure 2E, middle, and Supplemental Figure S3). Moreover, $PD1^+CD153^+$ cells colocalized with OPN^+ cells, and cGVHD mice had significantly more of these cells per field than control mice (Figure 2E, middle). To further examine LG fibrosis, we performed immunostaining for fibroblast markers, including the collagen-binding chaperone HSP47[19] and the terminally differentiated fibroblast marker α-SMA.[42,45] cGVHD LGs had more $HSP47^+$ and α-SMA^+ cells per field than control LGs (Figure 2E, right), suggesting that a subpopulation of abnormally activated and proliferative premature fibroblasts contribute to the severe fibrosis in cGVHD LGs, wherein mature fibroblasts abnormally transformed into senescent myofibroblasts. Taken together, these findings suggest that macrophages in cGVHD-affected regions activate the DDR, senesce, undergo cell cycle arrest, and produce SASP factors.

Cultured fibroblasts derived from cGVHD LGs showed higher 53BP1 and Ki-67 expression and HSP47 staining intensity than those from control LGs (Supplemental Figure S4), suggesting that a subpopulation of fibroblasts sustain DNA damage but remain activated and proliferate. Collectively, these findings indicate that IL-6, CXCL9, and OPN may be important SASP-related molecules in the pathology of cGVHD in LGs.

3.3 | Stress-induced senescence is partially associated with the pathology of cGVHD

To further confirm the association between cellular senescence and cGVHD, we used ABT-263 (Navitoclax), a potent senolytic agent that inhibits the anti-apoptotic activity of Bcl-2 family proteins, selectively induces apoptosis, and eliminates senescent cells by activating the proapoptotic proteins Bax and Bak, causing mitochondrial fusion as the apoptotic response to cellular stress.[15,28,32,33] The allogeneic BMT recipient mice were divided into 2 groups, which were treated with ABT-263 or vehicle only by gavage once daily for 7 days from days 10 to 16 after BMT (Figure 3A). To validate the mechanism of drug action on Bcl-2/Bax/Bak in LG tissue, we evaluated activated BAX, cleaved caspase-3 and fragmented DNA (TUNEL-positive) levels (Figure 3B and Supplemental Figure S5). ABT-263 significantly and dose-dependently increased the numbers of activated BAX^+ cells, cleaved caspase-3^+ cells and $TUNEL^+$ cells. There was no difference in body weight between the two groups (Figure 3C). To assess the function of cGVHD LGs, we measured the tear secretion volume, which was significantly higher 4 weeks after BMT in ABT-263-treated mice than in vehicle-treated mice (Figure 3D). In contrast to vehicle-treated mice, ABT-263-treated mice showed no blepharitis or diffuse corneal epithelitis (Figure 3E). Pathological analysis showed reduced inflammatory cell infiltration in the interstitial stroma of cGVHD LGs (Figure 3F) and skin (Supplemental Figure S6) in mice treated with 25 or 50 mg/kg ABT-263 (Figure 3F). The fibrotic LG area per field was significantly smaller in ABT-263-treated mice than in vehicle-treated mice, and this effect was dose-dependent (Figure 3G). Ultrastructural images of the LGs revealed fewer inflammatory cells (Figure 3H, left, and I) and collagen fibers (Figure 3H, middle) in the stroma and better preserved mitochondrial structures (Figure 3H, right) in ABT-263-treated mice than in vehicle-treated mice, suggesting that ABT-263 has a beneficial effect in cGVHD LGs. These data suggest that stress-induced senescence contributes to the pathogenesis of cGVHD in LGs. Cdkn2a

(p16) and Cxcl9 gene expression in LGs was significantly inhibited in ABT-263-treated mice compared with vehicle-treated mice (Supplemental Figure S7). The number of cells expressing the DDR marker 53BP1; the senescence markers p16 and p21; the SASP components IL-1β, IL-8, and IL-6; CD68; CD45; and HSP47 in the LG stroma was significantly lower in the ABT-263-treated cGVHD mice than in the vehicle-treated mice (Figure 4A). These findings indicate that the depletion of senescent cells may mitigate the effects of cGVHD on LGs. Interestingly, CXCL9 secretion in LG blood vessels was significantly suppressed in ABT-263-treated mice compared to vehicle-treated mice

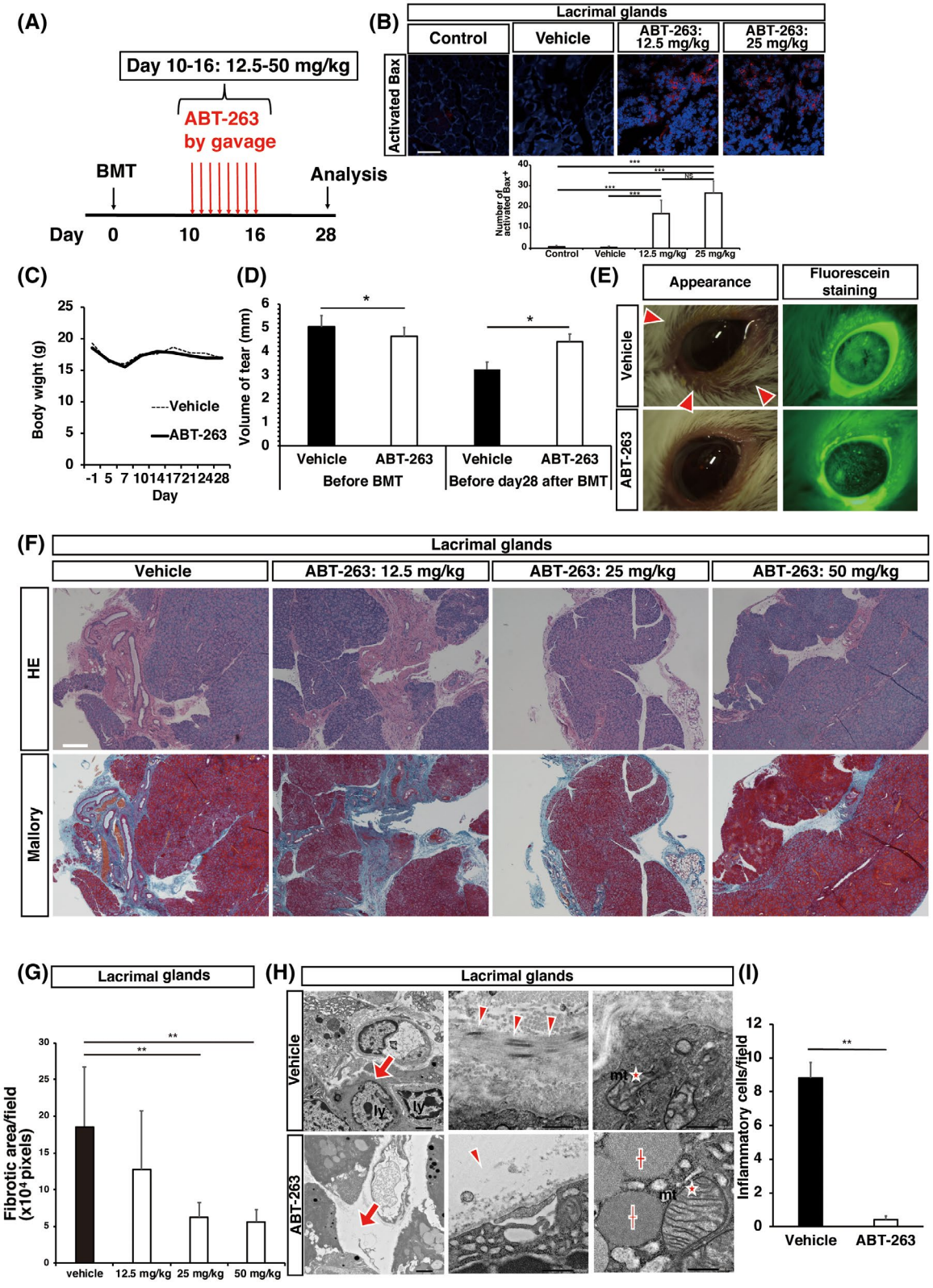

FIGURE 3 Cellular senescence contributes to cGVHD *A*, Schematic of the experimental treatment protocol with ABT-263, a potent senolytic and specific inhibitor of the antiapoptotic proteins BCL-2 and BCL-xL A and D, BMT, bone marrow transplantation. *B*, Dose-dependent increase in Bax (proapoptotic protein, red) expression in cGVHD LGs treated with ABT-263. *C*, Body weight of ABT-263- and vehicle-treated cGVHD mice (n = 5 per group). *D*, Mean tear volume in cGVHD mice treated with ABT-263 or vehicle (n = 5 per group). Data are presented as the mean ± SEM. $*P < .05$, unpaired Student's *t* test for ABT-263 versus vehicle and paired Student's *t* test for the vehicle group before vs after BMT *E*, Representative photographs of the cornea and eyelid (left) and fluorescein staining of the ocular surface (right) (n = 7 per group). Skin hair was lost around the eyelid of the vehicle-treated cGVHD mouse (red arrowheads). *F*, H&E and Mallory staining of LGs of ABT-263- and vehicle-treated cGVHD mice. Scale bar: 100 μm. *G*, Blue fibrotic areas identified by Mallory staining were measured by ImageJ software (n = 3 per group; 3 fields). Black bar: vehicle-treated group. White bar: ABT-263-treated group. Data are presented as the mean ± SEM. $**P < .01$, unpaired Student's *t* test. . *B-G*, Data are representative of two independent experiments. *H*, Electron microscopy analysis of LGs in ABT-263-treated (lower row) and vehicle-treated (upper row) cGVHD mice. Stromal areas in vehicle-treated cGVHD mice contain lymphocytes (upper left, red arrows) and collagen fibers (upper middle, red arrowheads), but those in ABT-263-treated cGVHD mice have no lymphocytes (lower left, red arrow) or collagen fibers with debris (lower middle, red arrowhead). Aberrant mitochondrial structures (upper right, red star) in vehicle-treated cGVHD mice. Mitochondria with normal cristae (lower right, red star) and secretory granules (lower right, red crosses) in ABT-263-treated cGVHD mice. Cap, capillary; ly, lymphocyte; Col, collagen; Mt, mitochondria. Scale bars: 2 μm (left) and 500 nm (middle and right). *I*, The number of infiltrated interstitial cells in the LGs per field (1225 μm^2) (n = 2 per group; 5 fields in total). Data are presented as the mean ± SEM. $**P < .01$, unpaired Student's *t* test

(Figure 4B), probably because this chemokine is a chemoattractant for macrophages and T cells in cGVHD-affected tissue.[53,54]

The number of $CD4^+$ T cells and $CD153^+$ T cells per field in LGs was significantly lower in the ABT-263-treated mice than in the vehicle-treated mice (Figure 4C, Supplemental Figure S8), indicating the senescence of some T cells in vehicle-treated cGVHD LGs. Senescent T cells were not detected in mice treated with 25 or 50 mg/kg ABT-263 (Supplemental Figure S8). Regulatory T cells remained in LGs of mice treated with 12.5-25 mg/kg ABT-263 (Supplemental Figure S9). Since 25 mg/kg ABT-263 improved fibrosis and inflammation better than 12.5 mg/kg ABT-263 (Figure 3F), the higher concentration was considered ideal in this cGVHD mouse model. We hypothesized that (1) senescent macrophages produce IL-6 and CXCL9, (2) CXCL9 recruits neighboring T cells in the microenvironment, and (3) IL-6 and/or CXCL9 promote the proliferation of an abnormal fibroblast subset damaged by various stresses.

To evaluate these hypotheses, we investigated how senescence aggravates cGVHD LGs. We focused on IL-6, since it is the most prominent SASP cytokine directly controlled by DDR signaling[25] and plays a critical role in cGVHD.[19,30,31] To confirm that SASP exacerbates cGVHD, we performed an inhibition experiment using the anti-mouse IL-6R mAb MR16-1. Allogeneic BMT recipient mice were divided into 2 groups that were treated with MR16-1 or PBS (vehicle control) by intraperitoneal injection 1 day before and 10, 17, and 24 days after BMT (Figure 5A). By day 28 after BMT, the vehicle-treated mice exhibited a cGVHD phenotype, including blepharitis, skin keratinization, rough fur, and diarrhea (Figure 5B). Notably, histological analysis revealed a significant reduction in excessive fibrosis in the LGs and skin of MR16-1-treated mice compared to vehicle-treated mice (Figure 5C,D). The findings in the vehicle group coincided with those in the sclerodermatous cGVHD mouse model (Figure 5B). Ultrastructural findings of the LG stroma showed lymphocytes and debris in vehicle-treated mice, which were scarce in MR16-1-treated mice (Figure 5E, left, and F). The basal lamina of the vascular endothelial cells in the LGs was thicker in vehicle-treated mice than in MR16-1-treated mice (Figure 5E, right).

Cdkn2a (p16) and Cdkn1a (p21) gene expression in cGVHD LGs was significantly lower in MR16-1-treated mice than in their vehicle-treated counterparts (Supplemental Figure S10). Il6 gene expression in cGVHD LGs tended to be lower in the MR16-1-treated group than in the vehicle-treated group (Supplemental Figure S10).

Next, we examined SASP-related protein levels in cGVHD LG tissues. There were no significant differences in the protein levels of DDR markers in LGs from the two groups (Figure 6A, left). On the contrary, consistent with the gene expression data (Supplemental Figure S10), the number of senescence biomarker-positive cells per field of LGs was significantly lower in the MR16-1-treated mice than in the control mice (Figure 6A, middle). Increased Cdkn2a mRNA and p16 protein levels are reported to enhance Cdkn2a mRNA stability in replicative senescence,[55] suggesting that IL-6 signaling blockade inhibits senescent cells from infiltrating the stroma in cGVHD LGs. There were more cells expressing proliferative cell markers in MR16-1-treated mice than in control mice (Figure 6A, right). MR16-1 treatment did not suppress the induction of apoptosis or upstream SASP-related molecule expression in cGVHD LGs (Figure 6B, left), suggesting that IL-6 is downstream of caspase-1 and IL-8. There were significantly fewer $IL\text{-}6^+$ cells and macrophages in the cGVHD LG stroma in the MR16-1-treated group than in the control group (Figure 6B, middle). MR16-1 significantly reduced the number of $HSP47^+$ cells per field in the MR16-1-treated

group compared to the vehicle group (Figure 6B, right), suggesting that IL-6 is a SASP molecule that aggravates cGVHD-related fibrosis. CXCL9 and OPN expression in endothelia and on vessel surfaces were significantly decreased in MR16-1-treated cGVHD LGs compared to vehicle-treated controls (Figure 6C), suggesting that CXCL9 and OPN are downstream of IL-6. A high magnification view of the images in Figure 6C revealed the localization of CXCL9 and OPN in the capillary lumen (Figure 6D). Collectively, these data suggest that IL-6 promotes senescence features in cGVHD.

To pursue mechanistic insight into the findings of this study, we cocultured various donor- and recipient-originated T cells with macrophages from the spleen of cGVHD

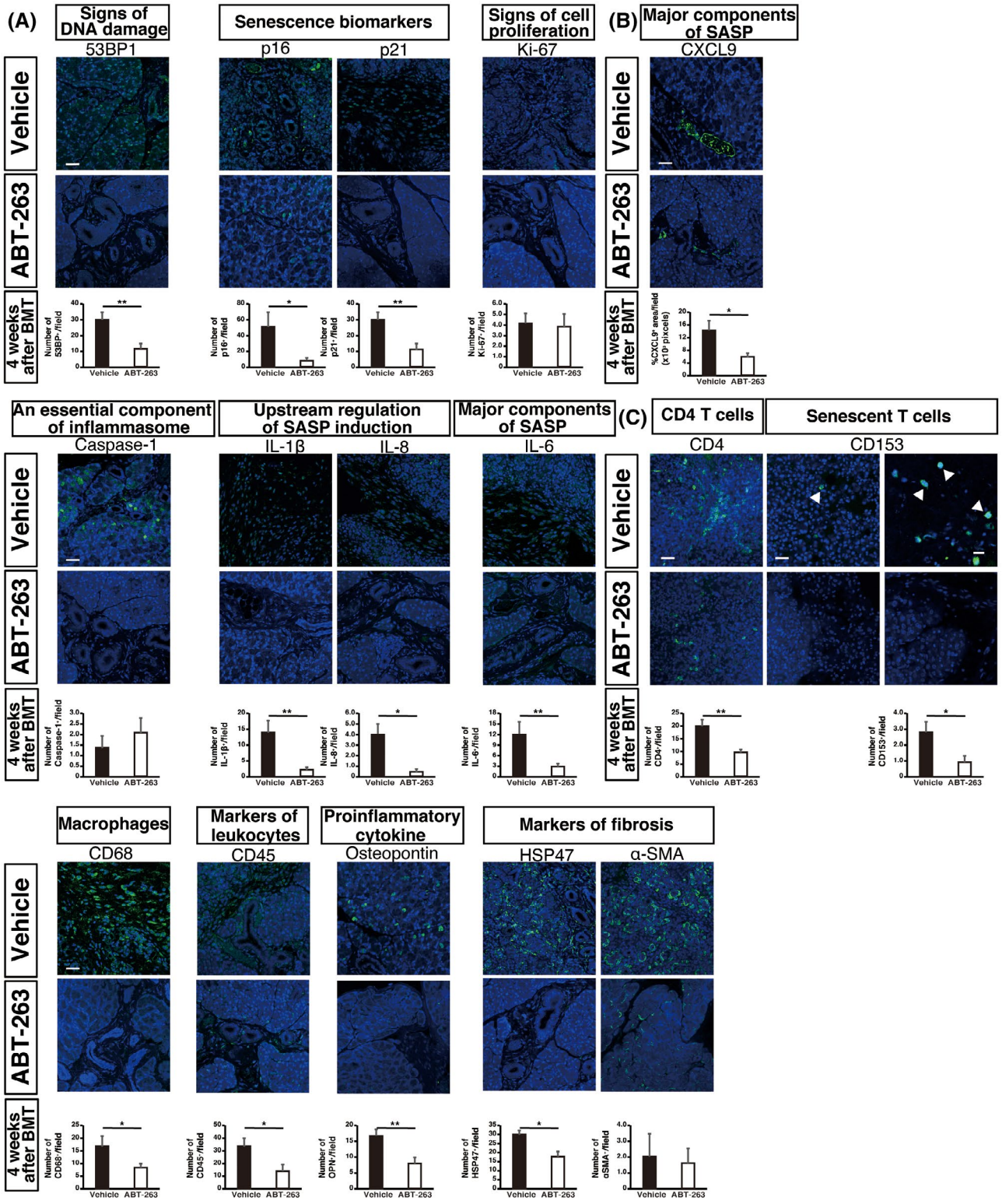

FIGURE 4 Effects of ABT-263 in the cGVHD lacrimal gland. *A-C*, Lacrimal gland (LG) sections from ABT263- and vehicle-treated mice 4 weeks after bone marrow transplantation (BMT) were stained for 53BP1 (DNA damage response, A upper low), p16 and p21 (senescence, *A* upper low), Ki-67 (proliferation, *A* upper low), caspase-1 (inflammasome component, *A middle low*), IL-1β and IL-8 (upstream indicators of SASP induction, *A* middle low), IL-6 (SASP component, *A* middle low), CD68 (macrophages, *A* lower low), CD45 (leukocytes, *A* lower low), osteopontin (OPN) (proinflammatory cytokine and SASP, *A* lower low), and HSP47 and α-SMA (fibrosis, *A* lower low) (green), and CD4 and CD153 (T cell and senescent T cell, *C*). The number of target (except OPN)-positive cells per field in the stroma and of OPN^+ cells per field on acini from the ABT-263-treated mice (n = 5) and the controls (n = 8) (> 5 fields per sample) 4 weeks after BMT *B,* Representative images of CXCL9, a SASP molecule, in LGs from ABT-263- and vehicle-treated mice 4 weeks after BMT. Green areas indicate $CXCL9^+$ secretion from vascular endothelia measured by Image J software (n = 3-4 per group;> 5 fields per sample). *A - B* Scale bar, 50 μm. *C*, Senescent $CD4^+$ (green) and $CD153^+$ T cells (green) among inflammatory cells in the lobules and stroma in LGs from ABT-263-treated mice (n = 7) and controls (n = 9) 4 weeks after BMT. The number of $CD4^+$ and $CD153^+$ cells per field from ABT-263-treated and control mice (> 5 fields per sample). Representative images of $CD153^+$ cells in LGs from control mice (white arrowheads) are shown. Scale bars: 50 μm (left and middle) and 20 μm (right). *A-C*, DAPI stains nuclei in blue. Data are representative of two independent experiments and presented as the mean ± SEM. **P* < .05, ** *P* < .01, unpaired Student's *t* test. ABT-263, a potent senolytic, is a specific inhibitor of the antiapoptotic proteins BCL-2 and BCL-xL

or syngeneic control mice (Figure 7A). Flow cytometry revealed that IL-6^+p16^+ macrophages were predominantly derived from cGVHD mice compared to syngeneic controls (Figure 7B). Among the cocultures, IL-6^+p16^+ macrophages from cGVHD mice were the most senescent upon coculture with T cells from cGVHD recipients. In addition, cGVHD macrophages interacting with recipient T cells (wild-type BALB/c T cells) expressed IL-6 and p16, suggesting that donor-derived $p16^+$ senescent macrophages may activate recipient T cells as antigen-presenting cells, leading to IL-6 production in the cGVHD LG microenvironment.

3.4 | SASP-related molecules associated with clinical findings in human cGVHD

To evaluate the clinical implications of our findings, we examined clinical samples. Patients with severe cGVHD often show ocular changes associated with senescence, including poliosis and conjunctival carcinoma.[22] We hypothesized that the T cell immune response and stress-induced senescence accelerate chronic ocular GVHD, resulting in excessive ocular fibrosis such as symblepharon and fornix shortening in cGVHD patients (Figure 8A).

To investigate whether stress-induced senescence is related to cGVHD progression in human LGs, we performed immunofluorescence analyses. 53BP1, IL-8, and IL-6 were highly expressed around the ducts and associated with many inflammatory cells in human cGVHD LGs compared to IgG4-related disease LGs (disease control) (Figure 8A,B).

The distributions of these molecules were different between the two groups. IL-6 was expressed on fibroblastic cells in cGVHD LGs but not in IgG4 tissue, whereas endothelia in both diseases expressed IL-6. Serum IL-6 levels were higher in chronic ocular GVHD patients than in those without chronic ocular GVHD (Figure 8C), suggesting that DDR activation and SASP molecules contribute to cGVHD LG in humans.

4 | DISCUSSION

Here, we demonstrated that the pathogenesis of cGVHD in affected LGs is partially associated with stress-induced senescence through the SASP evoked by senescent cells, although cGVHD is initiated by T cell-mediated immune responses.[5] The chronic ocular GVHD-associated secretory phenotype and SASP have similarities and overlapping components,[56] especially IL-1β, IL-8, CXCL1, IL-6, CXCL9, and OPN.

The gene and protein expression levels observed in our study suggest that a subset of macrophages, T cells, and fibroblasts senesce in response to DNA damage. The DDR starts with the recognition of DNA double-strand breaks by ɤ-H2A.X and amplified chromatin modifications by 53BP1. Simultaneously, the DDR facilitates cell cycle checkpoints and activates cyclin-dependent kinase inhibitors, including p16 and p21. When the DNA lesions are irreparable, the cells undergo permanent growth arrest (senescence) or apoptosis (death) involving caspase-1 and IL-1β expression. SASP reinforces senescence in cells damaged by various stresses. Senescent cells secrete factors such as IL-1β and IL-8 as upstream mediators of SASP in the early phase,[47] CXCL1 at three weeks after BMT, IL-6 at four weeks after BMT,[29] and CXCL9 and OPN as downstream components of IL-6, subsequently accelerating cellular senescence, and finally, leading to senescent changes, including cGVHD-related fibrosis.[23,56] Therefore, senescent cells with DNA damage produce SASP factors similar to late extracellular DDR signals.[57]

Senescent macrophages promote inflammation-driven angiogenesis in several age-related diseases, including atherosclerosis and age-related eye disease.[58] Our data suggest that senescent macrophages in the host environment are among the crucial origin cells that produce excessive SASP factors (Figure 2A-E).

Notably, a recent report showed that administering ABT-263 to either sublethally irradiated or chronologically aged mice effectively depletes senescent cells, thereby reducing TBI-induced premature aging of the hematopoietic system and rejuvenating aged hematopoietic stem cells in

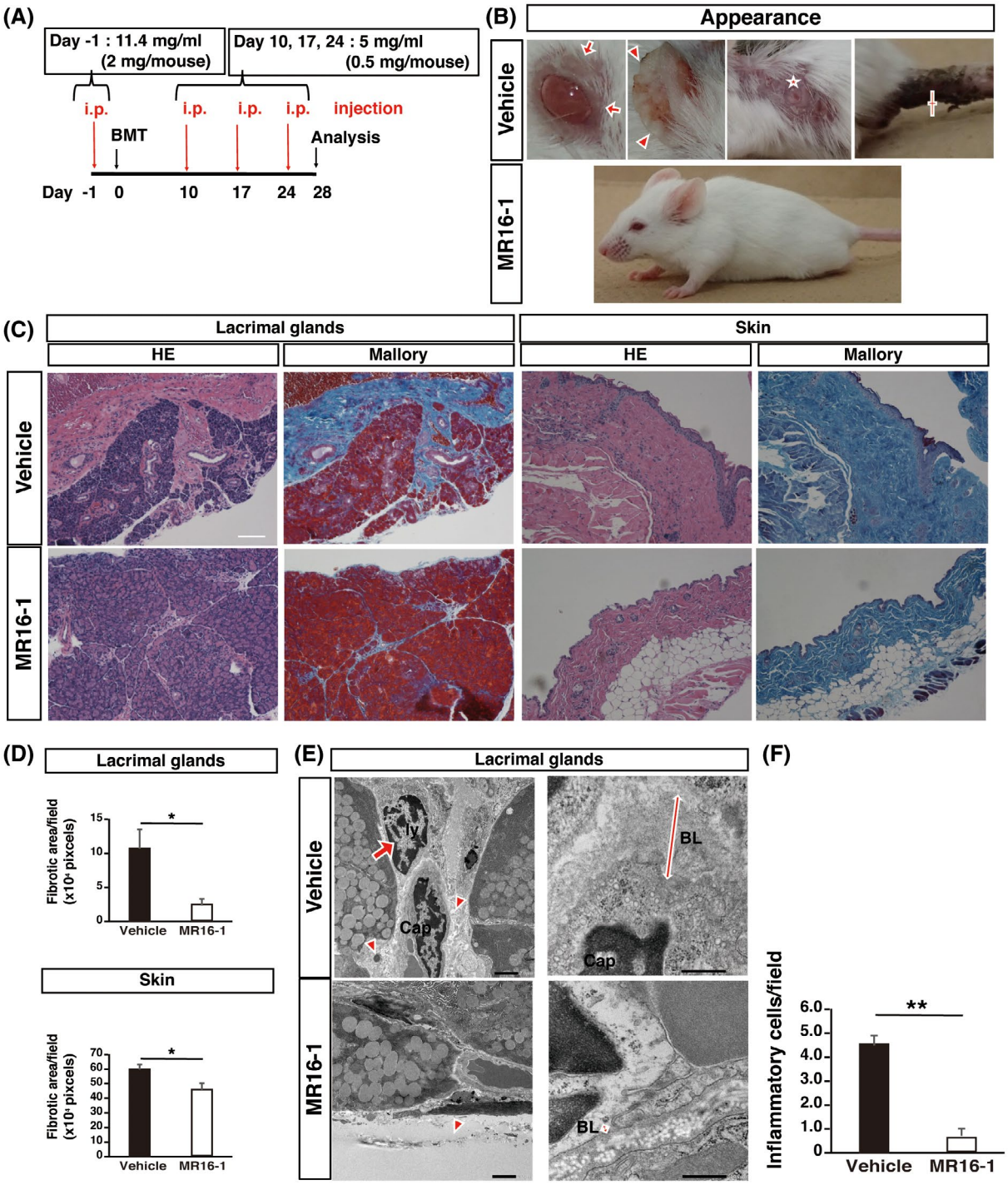

FIGURE 5 Blockade of IL-6, a major SASP factor, alleviates cGVHD. *A*, Schematic of the experimental treatment protocol for MR16-1, an anti-mouse IL-6 receptor monoclonal antibody. BMT, bone marrow transplantation. *B*, Representative photographs of MR16-1-treated and vehicle-treated cGVHD mice. The control mice exhibited cGVHD phenotypes such as blepharitis (red arrow), skin keratinization (red arrowheads), rough fur (red star), and diarrhea (red cross). The MR16-1-treated mice did not show cGVHD phenotypes. *C*, H&E and Mallory staining of lacrimal glands (LGs) and skin from MR16-1-treated and vehicle-treated cGVHD mice. *D*, Blue fibrosis areas identified by Mallory staining were measured by ImageJ software (n = 3 per group; 3 fields). Data are presented as the mean ± SEM. $*P < .05$, unpaired Student's *t* test. Scale bar, 100 μm. *B-D*, Data are representative of two independent experiments. *E*, Electron microscopy analysis of LGs from MR16-1- and vehicle-treated cGVHD mice. Stromal areas in vehicle-treated cGVHD mice contain lymphocytes (upper left, red arrow) and debris (upper left, red arrowheads), which are scarce in MR16-1-treated mice (lower left, red arrowhead). The basal lamina of vascular endothelial cells was thickened in vehicle-treated cGVHD mice (upper right, red arrow) compared to ABT-263-treated mice (lower right, red arrow). Cap, capillary; ly, lymphocyte; BL, basement lamina. Scale bars: 2 μm (left) and 500 nm (right). F, The number of infiltrated interstitial cells in the LGs per field (1225 μm^2) (n = 3 per group; 4 fields in total). Data are presented as the mean ± SEM. $**P < .01$, unpaired Student's *t* test

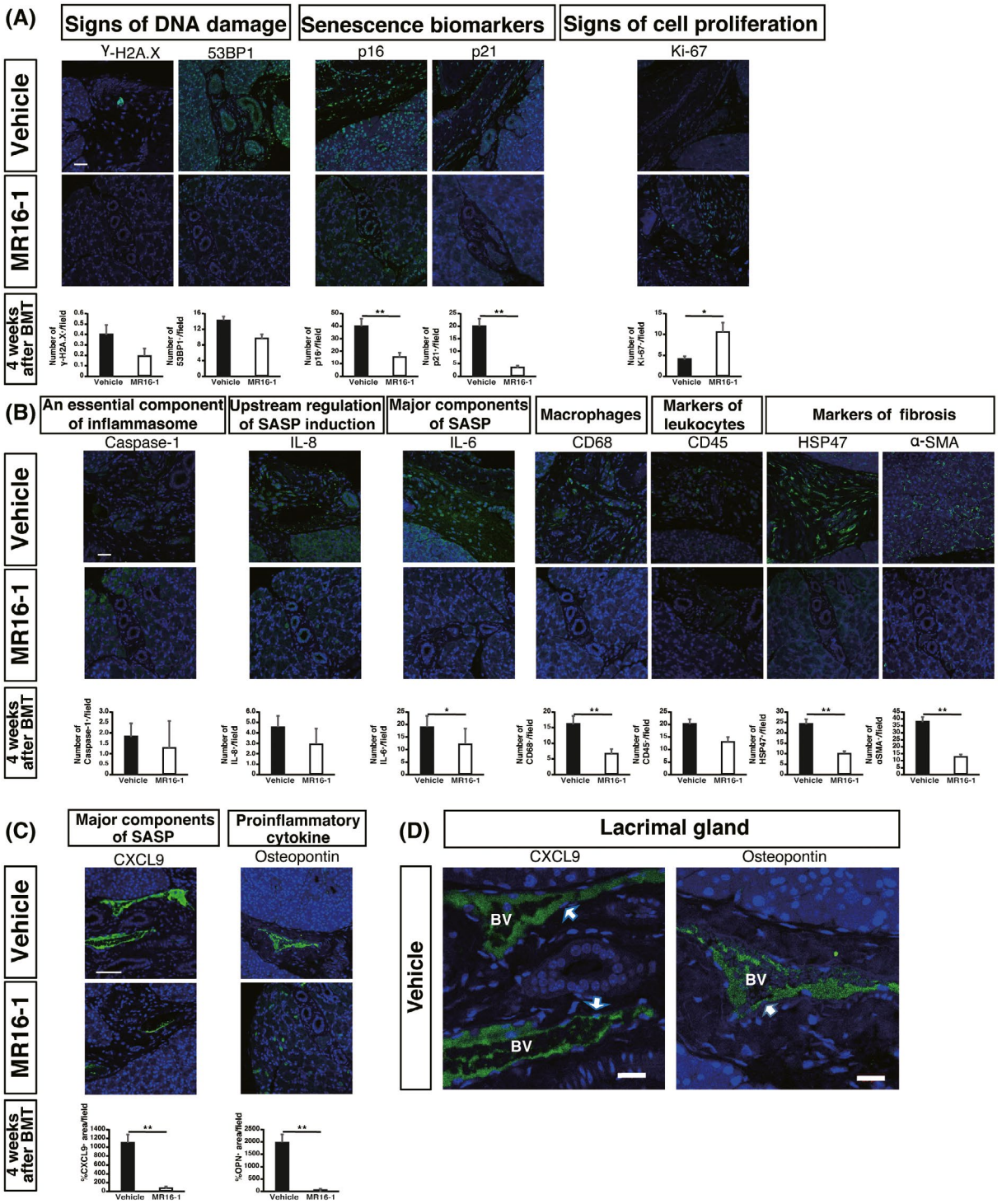

FIGURE 6 MR16-1 reduces the protein expression of senescence biomarkers and SASP-related molecules in cGVHD lacrimal glands. *A-B*, Lacrimal gland (LG) sections from MR16-1- and vehicle-treated mice 4 weeks after bone marrow transplantation (BMT) were stained for γ-H2A.X and 53BP1 (DNA damage response), p16 and p21 (senescence), Ki-67 (proliferation), caspase-1 (inflammasome), IL-8 (upstream indicator of SASP induction), IL-6 (SASP component), CD68 (macrophages), D45 (leukocytes), and HSP47 and α-SMA (fibrosis) (green). The number of target (except OPN)-positive cells per field in the stroma and of OPN^+ cells per field in acini from MR16-1-treated and vehicle-treated mice (n = 5 per group; >5 fields). Data are presented as the mean ± SEM. **P* < .05, ** *P* < .01, unpaired Student's *t* test. Scale bar: 50 μm. *C*, Representative images of CXCL9 (major SASP component) and OPN (proinflammatory cytokine) in the LGs of MR16-1- and vehicle-treated mice 4 weeks after BMT. Green areas indicating secretion (CXCL9 or OPN) from vascular endothelia were measured by ImageJ software (n = 5 per group;> 5 fields). Data are presented as the mean ± SEM. ***P* < .01, unpaired Student's *t* test. Scale bar: 50 μm. *D*, Representative images of CXCL9 or OPN inside endothelia (white arrows) in the stroma of cGVHD LGs from vehicle-treated control mice 4 weeks after BMT. BV, blood vessel. Scale bar: 20 μm. *A-D*, DAPI stains nuclei blue. MR16-1, anti-mouse IL-6 receptor monoclonal antibody

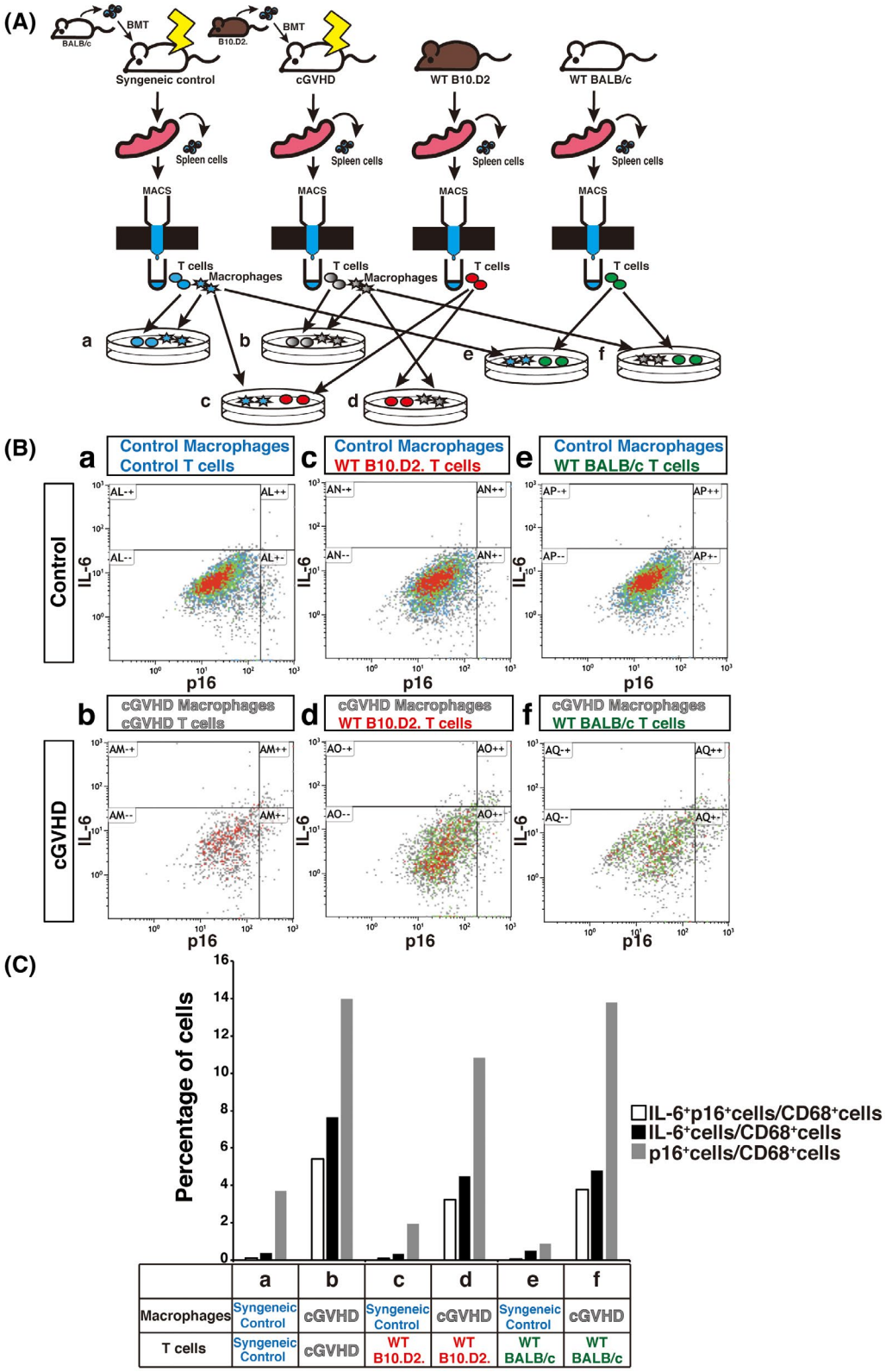

FIGURE 7 Cocultures of macrophages and T cells from various spleen sources. *A*, Cellular source of macrophages and T cells from spleen for cocultures. Macrophages and T cells from syngeneic controls (blue), cGVHD mice (gray), wild-type B10.D2 mice (red), and wild-type BALB/c mice (green). *B*, Flow cytometry analyses after coculture of macrophages and T cells from various sources. WT, wild-type. *C*, Percentages of IL-6^+p16^+ (white bar), IL-6^+ cells (black bar), and $p16^+$ cells (gray bar) among cocultured $CD68^+$ macrophages . Syngeneic controls (n = 4), cGVHD mice (n = 4), wild-type B10.D2. mice (n = 4), and wild-type BALB/c mice (n = 4). Data analysed at 4 weeks after BMT for syngeneic and cGVHD mice.

chronologically aged mice.[32] To validate the effects of ABT-263 on Bcl-2/Bax/Bak in LGs, we analyzed several molecules, including activated Bax and cleaved caspase-1, and performed TUNEL staining to determine whether this drug increases apoptosis in LG tissues. Activated Bax, cleaved caspase-1, and fragmented DNA (TUNEL staining) increased in a dose-dependent manner, indicating that ABT-263 can effectively induce apoptosis. Based on these results, we further assessed whether ABT-263 effectively eliminates senescent cells in cGVHD LGs and reduces cGVHD pathology. This senolytic drug, which specifically inhibits the antiapoptotic proteins BCL-2 and BCL-xL, removed senescent cells, including macrophages, T cells, and fibroblasts, in this cGVHD mouse model (Figure 4*A*,*C*). This clearance of senescent cells ameliorates the negative effects of cGVHD (Figure 3B-I) and suppresses the protein levels of DDR and

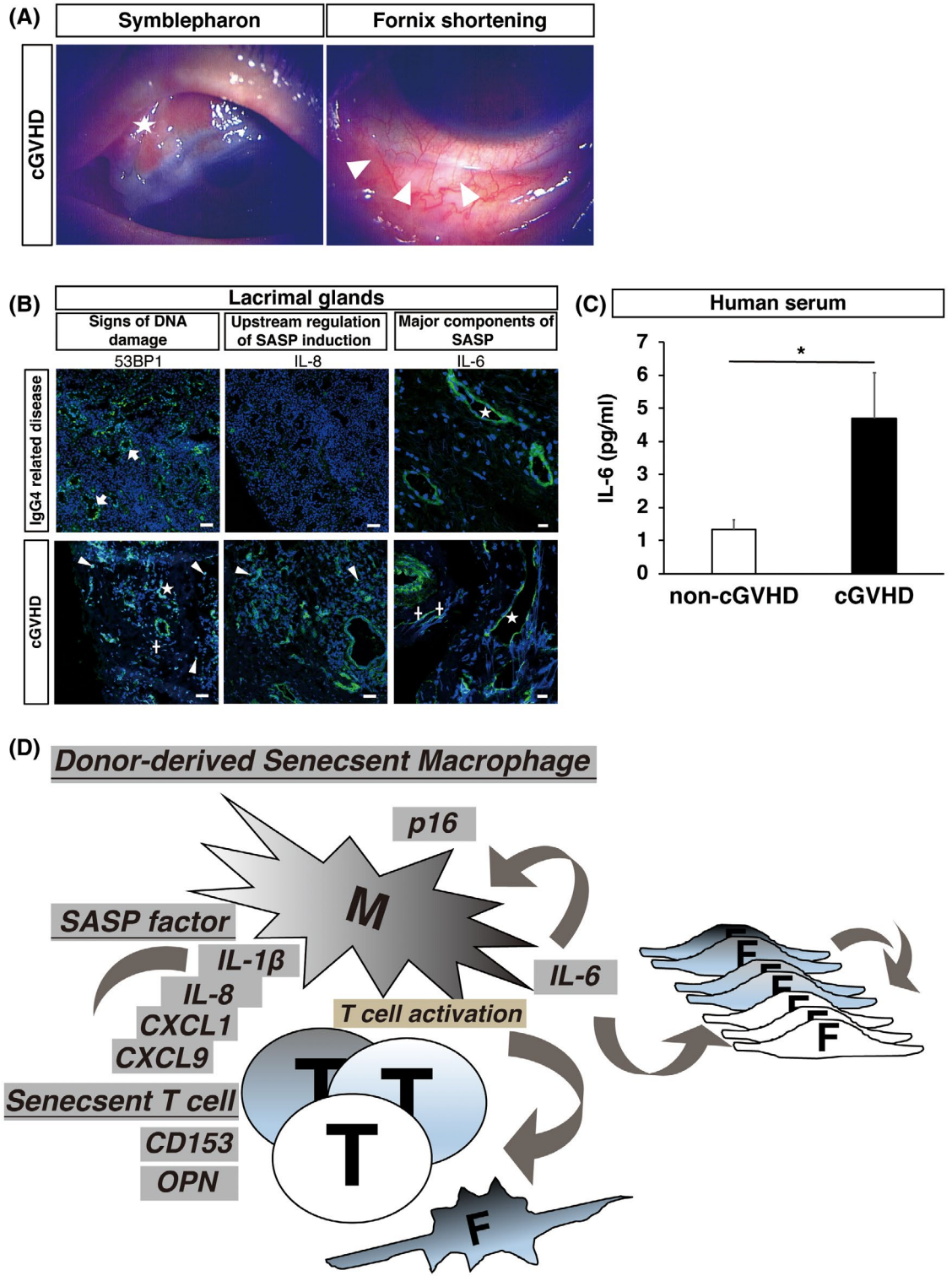

FIGURE 8 Characteristics of the ocular surface and lacrimal glands in human cGVHD and hypothetical model of pathogenic process in chronic ocular GVHD. *A*, Photographs from a cGVHD patient (58 yearsold, female) with symblepharon (white star) and fornix shortening (white arrowhead). *B*, Immunostaining for the DNA damage response marker 53BP1 (green), and senescence-associated secretory phenotype (SASP)-related molecules, IL-8 and IL-6 (green), in the stroma around ducts in cGVHD lacrimal glands (LGs) and IgG4-related disease LGs as a disease control. 53BP1, IL-8, and IL-6 positive cells in the stroma of the cGVHD LGs. $53BP1^+$ ductal epithelial cells (white arrows) and $IL\text{-}6^+$ endothelial cells (white star) are shown in the IgG4-related disease LGs. $53BP1^+$ endothelial cells (white star), interstitial fibroblast (white cross), and interstitial cells (white arrowheads), $IL\text{-}8^+$ interstitial cells (white arrowheads), and $IL\text{-}6^+$ endothelial cells (white star) and interstitial fibroblast (white crosses) are shown in the cGVHD LGs. DAPI stains nuclei in blue. Scale bars: 50 μm (53BP1 and IL-8) and 20 μm (IL-6). *C*, IL-6 levels in the serum of humans from the cGVHD and the non-cGVHD controls (cGVHD, n = 15, male = 7, female = 8, average age = 51.6 y/o; non-cGVHD controls, n = 7, male = 2, female = 5, average age = 47.7 y/o). Data indicate means ± SEM. $*P < .05$ by unpaired Student's *t* test. *D*, Schematic of the hypothetical model of chronic ocular GVHD pathogenesis. Several stressors cause cell cycle arrest. Macrophages exposed to severe damage undergo senescence and produce the SASP factors IL-6, CXCL1 and CXCL9 followed by IL-1β and IL-8. Then, IL-6 reinforces macrophage senescence in an autocrine manner. CXCL9 facilitates the recruitment of neighboring T cells to the microenvironment early after disease onset. Senescent T cells may accelerate stress-induced senescence as a late complication of cGVHD. Osteopontin (OPN) is a SASP factor that promotes epithelial-mesenchymal transition in cGVHD LGs. Consequently, a subset of senescent/mature fibroblasts, macrophages and T cells begin to synthesize abnormal collagens and extracellular matrix, leading to inflammation and abnormal fibrosis in cGVHD LGs

senescence biomarkers and SASP factors (Figure 4*A*-*C*), suggesting that ABT-263 partially abrogates the negative effects of stress-induced senescence in cGVHD. We propose that 25 mg/kg ABT-263 is the ideal dose in this cGVHD mouse model based on the maintenance of LG structures, depletion of $CD4^+CD153^+OPN^+$ senescent T cells, and preservation of $Foxp3^+$ regulatory T cells.

Next, since SASP factors are the major downstream paracrine signals of cellular senescence,[25,28] we demonstrated that IL-6 is one important SASP molecule in cGVHD (Figure 1D-F and 2B-E).

Inhibiting IL-6 may negate the stable activation of p16[55] and p21 (Figure 6A; Supplemental Figure S5A), lead to the reduced secretion of SASP factors, including CXCL9 and OPN (Figure 6C), and suppress cGVHD-triggered inflammation and fibrosis (Figures 5*B*-*F* and 6B). These data support the hypothesis that cellular senescence induced by IL-6, a canonical SASP component, promotes cGVHD-related fibrosis. Furthermore, we observed that the basal lamina of vascular endothelial cells in cGVHD LGs was thicker in the vehicle-treated group than the MR16-1-treated group (Figure 5E). This thickened basal lamina may result from exhaustion due to repeated damage and repair of the vessel walls,[43] as senescent macrophages (Figure 2B-D) and $CD3^+$ or $CD154^+$ T cells (Supplemental Figure S1A,B) in the host microenvironment may frequently infiltrate LG tissues from blood vessels. Senolysis and the inhibition of IL-6 signaling may relieve the abnormal T cell migration through vascular endothelial cells induced by CXCL9 (Figures 4B and 6C).

This study had some limitations. First, additional investigations are required to further characterize the DDR in specific cells in cGVHD. However, more specific, sensitive, and timely markers of the DDR are needed for these experiments.[56] Second, considering this is an in vivo cGVHD mouse model, it is difficult to accurately detect proliferating and nonproliferating cells. Third, IL-6 is a key molecule at the intersection of immune response mediators from immunocompetent cells and SASP factors from senescent cells; thus, it is necessary to separate these processes and study them individually. Further studies, such as those involving the depletion of senescent macrophages, T cells, or fibroblasts and the analysis of specific cultured cells, are required to determine the origin of SASP-producing senescent cells and to analyze the molecular mechanisms and signal transduction of SASP components underlying the time-dependent changes in cGVHD LGs and other target organs.

Based on these findings, we propose the following model for the pathogenesis of cGVHD in LGs (Figure 8D). Several stressors arrest the cell cycle, and macrophages exposed to severe damage undergo senescence and produce the SASP factors IL-6 and CXCL9 upon interacting with $CD4^+OPN^+CD153^+$ senescent T cells. Then, IL-6, a major driver of the SASP, reinforces macrophage senescence in an autocrine manner. In addition, CXCL9 facilitates the recruitment of neighboring T cells to the microenvironment early after onset.[53] T cell senescence after HSCT was recently reported in an acute GVHD animal model.[59] These senescent $CD4^+OPN^+CD153^+$ T cells may accelerate stress-induced senescence as a late complication of cGVHD. Moreover, IL-6 may induce the senescence of a subpopulation of fibroblasts. In addition, OPN, another SASP factor, promotes epithelial-mesenchymal transition in cGVHD LGs.[44,50-52] As a result, a subset of senescent/mature fibroblasts synthesizes abnormal collagens. On the contrary, when IL-6 affects other fibroblasts in the host environment in response to stress, the fibroblasts are exposed to only moderate, not permanent, damage, and resume proliferation. These fibroblasts affected by macrophages and T cells also synthesize excessive abnormal collagens and extracellular matrix,[43,45] leading to inflammation and

abnormal fibrosis in cGVHD LGs. Collectively, our findings suggest that senescent cells with the SASP or cells with stress-induced senescent features contribute to the pathogenesis of cGVHD in the LG, although immunological inflammation is the major underlying mechanism. Inhibiting the SASP evoked by senescent cells may be a new clinically translatable strategy for attenuating the effects of cGVHD in LGs and other target organs.

ACKNOWLEDGMENTS

We thank Dr Shinichiro Imai, Dr Eiji Hara, and Dr Naoko Ohtani for their valuable suggestions and instructions. Our sincere appreciation is also given to Dr Toshihiro Nagai, Dr Tetsuya Yano, Dr Robert Rush, Dr Kenji Morii, Dr Shigeru Nakamura, Dr Toshihiro Imada, Mr Kazuki Asai and Dr Mai Tadaki for their excellent technical assistance. This work was supported by grants from the Japanese Ministry of Education, Science, Sports, Culture and Technology (26462668 and 18K09421) to Y. O., from Brain Mapping by Integrated Neurotechnologies for Disease Studies (Brain/MINDS) of the Japan Agency for Medical Research and Development (AMED) (JP178dm0207002) to S. Shibata and (JP178dm0207001) to H. O., from Program for the Advancement of Research in Core Projects under Keio University's Longevity Initiative (KGRI) to K. T. and M. H., and from Academic Development Project Grant-in-Aid by JSR Corporation 2019 to E. S.

CONFLICT OF INTEREST

Y. O., S. Shimmura, and H. O. received MR16-1 from Chugai Pharmaceutical Co., Ltd. M. Y., S. Sato, E. S., S. Shibata, M. H., T. Y., H.K., M.O., T. S., S. M., T. T., Y. K. declare neither financial nor nonfinancial conflicts of interest. Patent applied by Keio University (Japanese Patent Application No. 2019-004730. Inventor; Y. O., E. S., M.Y., and K.T.). There are no other relevant declarations relating to this patent. This does not alter our adherence to the policies on sharing data and materials. The other authors declare no competing interest associated with this manuscript.

AUTHOR CONTRIBUTIONS

M. Yamane, Y. Ogawa, and K. Tsubota designed the experiments. M. Yamane, S. Sato, E. Shimizu, H. Kamijuku, and Y. Ogawa conducted the experiments, M. Yamane, S. Sato, Y. Ogawa, E. Shimizu, S. Shibata, M. Hayano, H. Kamijuku, T. Yaguchi, M. Ogawa, T. Suzuki, S. Mukai, S. Shimmura, H. Okano, T. Takeuchi, Y. Kawakami, and K. Tsubota discussed and analyzed the data. M. Yamane, S. Sato, E. Shimizu, S. Mukai, and Y. Ogawa wrote the paper. All authors have read and agreed on the final version. Y. Ogawa and K. Tsubota supervised this study. Y. Ogawa, E. Shimizu, S. Shibata, H.O and K. Tsubota funded this study.

DATA AVAILABILITY STATEMENT

The data that support the findings of this study are available within the article and supplemental data or from the corresponding author upon reasonable request.

REFERENCES

1. Ferrara JL, Levine JE, Reddy P, Holler E. Graft-versus-host disease. *Lancet*. 2009;373:1550-1561.
2. Ogawa Y, Okamoto S, Wakui M, et al. Dry eye after haematopoietic stem cell transplantation. *Br J Ophthalmol*. 1999;83:1125-1130.
3. Ogawa Y, Shimmura S, Dogru M, Tsubota K. Immune processes and pathogenic fibrosis in ocular chronic graft-versus-host disease and clinical manifestations after allogeneic hematopoietic stem cell transplantation. *Cornea*. 2010;29(Suppl 1):S68-S77.
4. Lee SJ. Classification systems for chronic graft-versus-host disease. *Blood*. 2017;129:30-37.
5. MacDonald KP, Hill GR, Blazar BR. Chronic graft-versus-host disease: biological insights from preclinical and clinical studies. *Blood*. 2017;129:13-21.
6. Munir SZ, Aylward J. A review of ocular graft-versus-host disease. *Optom Vis Sci*. 2017;94:545-555.
7. Holtan SG, Pasquini M, Weisdorf DJ. Acute graft-versus-host disease: a bench-to-bedside update. *Blood*. 2014;124:363-373.
8. Perez VL, Barsam A, Duffort S, et al. Novel scoring criteria for the evaluation of ocular graft-versus-host disease in a preclinical allogeneic hematopoietic stem cell transplantation animal model. *Biol Blood Marrow Transplant*. 2016;22:1765-1772.
9. Ogawa Y, Kim SK, Dana R, et al. International chronic ocular graft-vs-host-disease (GVHD) consensus group: proposed diagnostic criteria for chronic GVHD (Part I). *Sci Rep*. 2013;3:3419.
10. Riemens A, te Boome L, Imhof S, Kuball J, Rothova A. Current insights into ocular graft-versus-host disease. *Curr Opin Ophthalmol*. 2010;21:485-494.
11. Sun YC, Chai X, Inamoto Y, et al. Impact of ocular chronic graft-versus-host disease on quality of life. *Biol Blood Marrow Transplant*. 2015;21:1687-1691.
12. Inamoto Y, Flowers ME. Treatment of chronic graft-versus-host disease in 2011. *Curr Opin Hematol*. 2011;18:414-420.
13. Ciceri F, Labopin M, Aversa F, et al. A survey of fully haploidentical hematopoietic stem cell transplantation in adults with high-risk acute leukemia: a risk factor analysis of outcomes for patients in remission at transplantation. *Blood*. 2008;112:3574-3581.
14. Socie G, Ritz J. Current issues in chronic graft-versus-host disease. *Blood*. 2014;124:374-384.
15. He S, Sharpless NE. Senescence in health and disease. *Cell*. 2017;169:1000-1011.
16. Toussaint O, Dumont P, Remacle J, et al. Stress-induced premature senescence or stress-induced senescence-like phenotype: one in vivo reality, two possible definitions? *ScientificWorldJournal*. 2002;2:230-247.
17. Min CK. The pathophysiology of chronic graft-versus-host disease: the unveiling of an enigma. *Korean J Hematol*. 2011;46:80-87.
18. Zhang Y, McCormick LL, Desai SR, Wu C, Gilliam AC. Murine sclerodermatous graft-versus-host disease, a model for human scleroderma: cutaneous cytokines, chemokines, and immune cell activation. *J Immunol*. 2002;168:3088-3098.
19. Ogawa Y, Morikawa S, Okano H, et al. MHC-compatible bone marrow stromal/stem cells trigger fibrosis by activating host T cells in a scleroderma mouse model. *Elife*, 5:e09394.

20. Yaguchi S, Ogawa Y, Shimmura S, et al. Angiotensin II type 1 receptor antagonist attenuates lacrimal gland, lung, and liver fibrosis in a murine model of chronic graft-versus-host disease. *PLoS One*. 2013;8:e64724.
21. Mukai S, Ogawa Y, Urano F, Kudo-Saito C, Kawakami Y, Tsubota K. Novel treatment of chronic graft-versus-host disease in mice using the ER stress reducer 4-phenylbutyric acid. *Sci Rep*. 2017;7:41939.
22. Kawai M, Ogawa Y, Shimmura S, et al. Expression and localization of aging markers in lacrimal gland of chronic graft-versus-host disease. *Sci Rep*. 2013;3:2455.
23. Minamino T, Orimo M, Shimizu I, et al. A crucial role for adipose tissue p53 in the regulation of insulin resistance. *Nat Med*. 2009;15:1082-1087.
24. Collado M, Serrano M. Senescence in tumours: evidence from mice and humans. *Nat Rev Cancer*. 2010;10:51-57.
25. Coppe JP, Desprez PY, Krtolica A, Campisi J. The senescence-associated secretory phenotype: the dark side of tumor suppression. *Annu Rev Pathol*. 2010;5:99-118.
26. van Deursen JM. The role of senescent cells in ageing. *Nature*. 2014;509:439-446.
27. Yoshimoto S, Loo TM, Atarashi K, et al. Obesity-induced gut microbial metabolite promotes liver cancer through senescence secretome. *Nature*. 2013;499:97-101.
28. Chiche A, Le Roux I, von Joest M, et al. Injury-induced senescence enables in vivo reprogramming in skeletal muscle. *Cell Stem Cell*. 2017;20(407-414):e404.
29. Rodier F, Coppe JP, Patil CK, et al. Persistent DNA damage signalling triggers senescence-associated inflammatory cytokine secretion. *Nat Cell Biol*. 2009;11:973-979.
30. Tvedt THA, Ersvaer E, Tveita AA, Bruserud O. Interleukin-6 in allogeneic stem cell transplantation: its possible importance for immunoregulation and as a therapeutic target. *Front Immunol*. 2017;8:667.
31. Barak V, Levi-Schaffer F, Nisman B, Nagler A. Cytokine dysregulation in chronic graft versus host disease. *Leuk Lymphoma*. 1995;17:169-173.
32. Chang J, Wang Y, Shao L, et al. Clearance of senescent cells by ABT263 rejuvenates aged hematopoietic stem cells in mice. *Nat Med*. 2016;22:78-83.
33. Zhu Y, Tchkonia T, Fuhrmann-Stroissnigg H, et al. Identification of a novel senolytic agent, navitoclax, targeting the Bcl-2 family of anti-apoptotic factors. *Aging Cell*. 2016;15:428-435.
34. Shoemaker AR, Mitten MJ, Adickes J, et al. Activity of the Bcl-2 family inhibitor ABT-263 in a panel of small cell lung cancer xenograft models. *Clin Cancer Res*. 2008;14:3268-3277.
35. Tawara I, Koyama M, Liu C, et al. Interleukin-6 modulates graft-versus-host responses after experimental allogeneic bone marrow transplantation. *Clin Cancer Res*. 2011;17:77-88.
36. Ohtani N, Imamura Y, Yamakoshi K, et al. Visualizing the dynamics of p21(Waf1/Cip1) cyclin-dependent kinase inhibitor expression in living animals. *Proc Natl Acad Sci USA*. 2007;104:15034-15039.
37. Brack AS, Conboy MJ, Roy S, et al. Increased Wnt signaling during aging alters muscle stem cell fate and increases fibrosis. *Science*. 2007;317:807-810.
38. Schneider CA, Rasband WS, Eliceiri KW. NIH Image to ImageJ: 25 years of image analysis. *Nat Methods*. 2012;9:671-675.
39. Shirakawa K, Yan X, Shinmura K, et al. Obesity accelerates T cell senescence in murine visceral adipose tissue. *J Clin Invest*. 2016;126:4626-4639.
40. Ogawa Y, Kuwana M, Yamazaki K, et al. Periductal area as the primary site for T-cell activation in lacrimal gland chronic graft-versus-host disease. *Invest Ophthalmol Vis Sci*. 2003;44:1888-1896.
41. Cui Y, Li Q. Expression and functions of fibroblast growth factor 10 in the mouse mammary gland. *Int J Mol Sci*. 2013;14:4094-4105.
42. Yaguchi S, Ogawa Y, Shimmura S, et al. Presence and physiologic function of the renin-angiotensin system in mouse lacrimal gland. *Invest Ophthalmol Vis Sci*. 2012;53:5416-5425.
43. Ogawa Y, Yamazaki K, Kuwana M, et al. A significant role of stromal fibroblasts in rapidly progressive dry eye in patients with chronic GVHD. *Invest Ophthalmol Vis Sci*. 2001;42:111-119.
44. Ogawa Y, Shimmura S, Kawakita T, Yoshida S, Kawakami Y, Tsubota K. Epithelial mesenchymal transition in human ocular chronic graft-versus-host disease. *Am J Pathol*. 2009;175:2372-2381.
45. Ogawa Y, Razzaque MS, Kameyama K, et al. Role of heat shock protein 47, a collagen-binding chaperone, in lacrimal gland pathology in patients with cGVHD. *Invest Ophthalmol Vis Sci*. 2007;48:1079-1086.
46. Yaguchi S, Ogawa Y, Kawakita T, Shimmura S, Tsubota K. Tissue renin-angiotensin system in lacrimal gland fibrosis in a murine model of chronic graft-versus-host disease. *Cornea*. 2015;34(Suppl 11):S142-S152.
47. Malaquin N, Martinez A, Rodier F. Keeping the senescence secretome under control: molecular reins on the senescence-associated secretory phenotype. *Exp Gerontol*. 2016;82:39-49.
48. Jankovic D, Ganesan J, Bscheider M, et al. The Nlrp3 inflammasome regulates acute graft-versus-host disease. *J Exp Med*. 2013;210:1899-1910.
49. Pazolli E, Alspach E, Milczarek A, Prior J, Piwnica-Worms D, Stewart SA. Chromatin remodeling underlies the senescence-associated secretory phenotype of tumor stromal fibroblasts that supports cancer progression. *Cancer Res*. 2012;72:2251-2261.
50. Uchibori T, Matsuda K, Shimodaira T, Sugano M, Uehara T, Honda T. IL-6 trans-signaling is another pathway to upregulate Osteopontin. *Cytokine*. 2017;90:88-95.
51. Kothari AN, Arffa ML, Chang V, et al. Osteopontin-A master regulator of epithelial-mesenchymal transition. *J Clin Med*. 2016;5:39.
52. Kawakami K, Minami N, Matsuura M, et al. Osteopontin attenuates acute gastrointestinal graft-versus-host disease by preventing apoptosis of intestinal epithelial cells. *Biochem Biophys Res Commun*. 2017;485:468-475.
53. Kitko CL, Levine JE, Storer BE, et al. Plasma CXCL9 elevations correlate with chronic GVHD diagnosis. *Blood*. 2014;123:786-793.
54. Arango Duque G, Descoteaux A. Macrophage cytokines: involvement in immunity and infectious diseases. *Front Immunol*. 2014;5:491.
55. Hornsby PJ. Stress-induced senescence. In: Sedivy M, Adams, PD, eds. *Cellular Senescence and Tumor Suppression*. New York, NY: Springer; 2010:85-106.
56. Wang WJ, Cai GY, Chen XM. Cellular senescence, senescence-associated secretory phenotype, and chronic kidney disease. *Oncotarget*. 2017;8:64520-64533.
57. Malaquin N, Carrier-Leclerc A, Dessureault M, Rodier F. DDR-mediated crosstalk between DNA-damaged cells and their microenvironment. *Front Genet*. 2015;6:94.
58. Sene A, Khan AA, Cox D, et al. Impaired cholesterol efflux in senescent macrophages promotes age-related macular degeneration. *Cell Metab*. 2013;17:549-561.

59. Beatty GL, Smith JS, Reshef R, et al. Functional unresponsiveness and replicative senescence of myeloid leukemia antigen-specific CD8+ T cells after allogeneic stem cell transplantation. *Clin Cancer Res*. 2009;15:4944-4953.

SUPPORTING INFORMATION

Additional supporting information may be found online in the Supporting Information section.

How to cite this article: Yamane M, Sato S, Shimizu E, et al. Senescence-associated secretory phenotype promotes chronic ocular graft-vs-host disease in mice and humans. *The FASEB Journal*. 2020;00:1–23. https://doi.org/10.1096/fj.201900218R